Temporal Changes of the Primary Circulation in Tropical Cyclones

H. E. WILLOUGHBY

Hurricane Research Division, AOML/NOAA, Miami, Florida

(Manuscript received 31 January 1989, in final form 6 September 1989)

ABSTRACT

More than 900 radial profiles of in situ aircraft observations collected in 19 Atlantic hurricanes and tropical storms over 13 years confirm that the usual mechanism of tropical cyclone intensification involves contracting maxima of the axisymmetric swirling wind. Radar shows that annuli of convective echoes accompany the wind maxima. These features, called convective rings, exist and move inward because latent heat released in the rings leads to descent, adiabatic warming, and rapid isobaric height falls in the area they enclose. The radial change in rate of isobaric height fall is concentrated at the inner edge of the wind maximum, causing the gradient wind to increase there and the maximum to contract. Vigorous convection organized in rings invariably causes well defined, inward moving wind maxima, but when convection is weak, the rings are also weak or even absent. In this case, the swirling wind may be nearly constant with radius and change slowly in time.

Hurricanes that have a single, vigorous, axisymmetric convective ring strengthen rapidly. Although a series of minor convective rings may support steady strengthening, development is more generally episodic. When asymmetric convection erupts near the center of tropical storms or weak hurricanes, it may cause intensification to falter and the cyclone tracks to become irregular. In intense hurricanes, outer convective rings may form around the preexistent eyewalls, contract, and strangle the original eyewalls, halting intensification or causing weakening.

1. Introduction

This paper deals with the observationally based convective ring model for temporal changes of the primary circulation—the axisymmetric swirling or tangential wind—in tropical cyclones. The model stems from the seemingly unusual behavior of three axisymmetric hurricanes with maximum wind (V_{max}) > 50 m s^{-1}: Anita of 1977, David of 1979, and Allen of 1980. The primary inner eyewalls of these hurricanes contracted as the hurricanes intensified. Simultaneously, convection outside the primary eyewalls became organized into rings that encircled the eyewalls and coincided with outer maxima of the swirling wind. Although Anita passed onshore soon after the outer eyewall formed, radar and in situ observations showed clearly that the outer convective rings in David and Allen constricted around the preexistent eyewalls and in time supplanted them. In Allen, three eyewall successions occurred, each of which caused a dramatic increase of central surface pressure and decrease of V_{max} (Willoughby et al. 1982; Marks 1985).

A statistical analysis of the in situ observations from Anita, David, and Allen was used to estimate the mean values and temporal rates of change for the swirling wind and isobaric height in hurricane-centered coordinates as functions of radius. The radial variation of the temporal change demonstrated kinematically that the radius of maximum wind (RMW) contracted because the wind strengthened most rapidly on the RMW's inward side. Since the strengthening usually extended across the RMW, V_{max} increased as the RMW moved inward. The isobaric height showed rapid falls within the RMW and slower falls outside it. The largest gradient of height fall lay inside the RMW where the wind increased most rapidly with time, as one would expect if the wind remained in gradient balance.

The gradient wind relation was, in fact, the key to understanding convective rings. A scale analysis (Willoughby 1979; Shapiro and Willoughby 1982) showed that gradient balance described the primary circulation when the secondary circulation—the axisymmetric radial and vertical motion—was small compared with the primary circulation. In a theoretical context, gradient balance allowed algebraic elimination of the time derivatives between the thermodynamic and tangential-momentum equations in order to form a single equation for the secondary flow induced by imposed heat or momentum sources (Eliassen 1952). Substitution of the diagnosed secondary circulation into the original equations yielded a description of the gradual evolution of the vortex (Smith 1981; Shapiro and Willoughby 1982; Schubert and Hack 1982).

The temporal changes thus calculated agreed with the observations: the wind strengthened at and inside the RMW. The sharp gradient of isobaric height tendency due to convective latent heat release coincided

Corresponding author address: Dr. Hugh E. Willoughby, NOAA/AOML/HRD, 4301 Rickenbacker Causeway, Miami, FL 33149.

with the most rapid wind strengthening. The gradient lay between the area inside RMW, where strong inertial resistance to horizontal motion concentrated compensating subsidence and adiabatic warming, and the area outside the RMW, where the inertial resistance to horizontal motion was weaker and adiabatic heating more diffuse. Moreover, the balanced model suggested that when two concentric convective rings were present, the outer would induce descent and upper tropospheric warming over the inner, thus supplanting it by choking off its convective instability.

The observations of Allen's intensity changes came at a time when it was generally believed that hurricanes maintained their intensity if they remained over the warm tropical sea (e.g., Riehl 1954). Only a few examples of concentric eyes could be documented, so that, despite a well-developed theory, no one knew how common they were or whether the convective ring model was a good description of hurricanes in general. The observations of the primary circulation and convection presented here confirm the contracting convective rings are common in vigorously convective hurricanes and that when $V_{max} \geq 45$ m s^{-1} concentric eyewalls often form, leading to eyewall succession within 12–36 h if landfall does not occur first. A companion paper (Willoughby 1990) addresses balance of the primary circulation.

2. Data and analysis

Table 1 summarizes the observations in this study. The data span more than a decade and contain 977 radial passes—penetrations or exits from the eye—observed during 84 aircraft sorties into 19 Atlantic tropical storms or hurricanes, making it 50% larger than that in Gray and Shea's (1973) landmark study.

In the text and figures, each aircraft sortie (a single flight by a single aircraft) is denoted by an identifier in which the first pair of digits is the year, the second pair is the month, and the third pair is the day UTC on which the flight began. The six digits are followed by a letter identifying the individual WP-3D aircraft, H for N42RF or I for N43RF, and sometimes by the number 2 denoting the second sortie by that aircraft on the day in question. Thus, 830817I2 identifies the second flight by aircraft N43RF on 17 August 1983. In flights when the aircraft remained in the air past 00 UTC, the flight identifier decodes to the day on which it took off, even if the observations were made the next day.

Important goals of the experimental design were uniform data coverage in space and time and accurate estimation of the temporally varying, axisymmetric meteorological fields. In each hurricane, the aircraft flew sequential sorties at constant altitude to measure temporal changes without confounding them with vertical variations. The flight tracks varied. In a few cyclones, they were perpendicular traverses oriented along cardinal directions across the circulation center; but in most cyclones, some traverses covered intermediate azimuths as well.

Limitations of aircraft range and duration, mechanical or electronic failures, and a prohibition against flying over land under hurricane conditions sometimes compromised uniform coverage. Figure 1 illustrates how the last of these factors affected operations during four sorties in Hurricane Alicia. When Alicia was well at sea, the coverage was excellent; the passes were

TABLE 1. Sorties and radial passes flown in the tropical cyclones in this study.

	Cyclone	Year	Number of sorties	Passes				
				900 mb	850 mb	700 mb	500 mb	Total
1	Anita	1977	1			20		20
2	David	1979	3		24			24
3	Frederic	1979	6	18	32	2	10	62
4	Allen	1980	7		32	46	31	109
5	Gert	1981	6		78			78
6	Alicia	1983	4		50			50
7	Arthur	1984	3	22				22
8	Diana	1984	10	48	80			128
9	Danny	1985	3		26			26
10	Elena	1985	9		142			142
11	Gloria	1985	7		34	10	6	50
12	Isabel	1985	4		48			48
13	Juan	1985	4		36			36
14	Charley	1986	3	28				28
15	Emily	1987	3			18	38	56
16	Floyd	1987	2	10	12			22
17	Florence	1988	2	20				20
18	Gilbert	1988	6		22	28		50
19	Joan	1988	1		6			6
Total			84	146	622	124	85	977

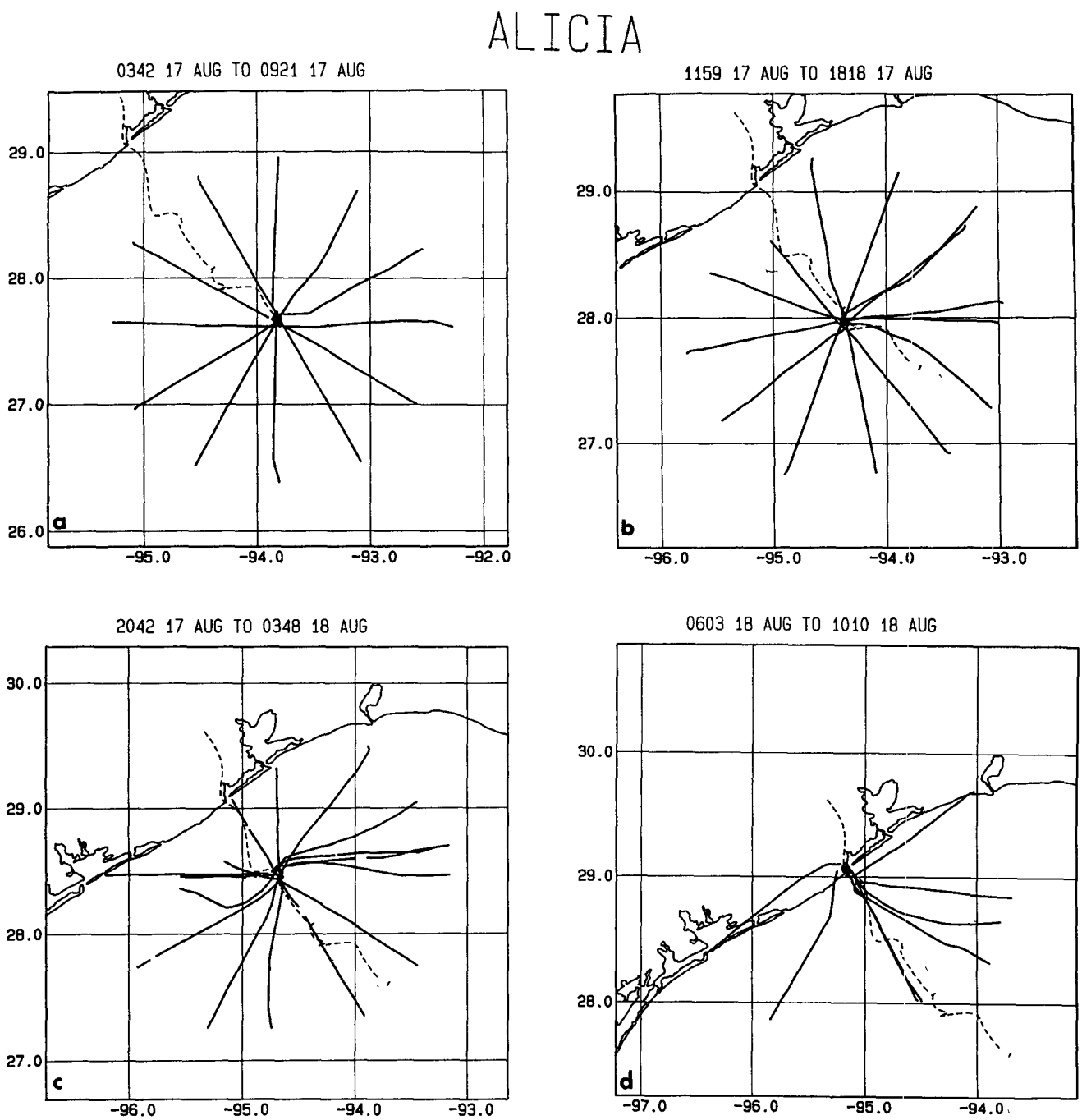

FIG. 1. The dashed curve is the track of Hurricane Alicia of 1983. The heavy solid curves show the cyclone-relative aircraft track during the radial passes illustrating: (a) excellent data coverage, flight 830817I; (b) good data coverage, flight 830817H; (c) fair data coverage, flight 830817I2; and (d) poor data coverage, flight 830818H.

spaced equally in azimuth and nearly the same length. As Alicia approached the coast, the coverage became good, then fair, as passes clustered on the east side and those on the landward side were shortened to avoid the shore. Finally at landfall, the coverage was poor, with radial passes confined to the semicircle of the vortex that remained over water. The data presented in this paper represent fair coverage or better. In some cases, the domain was made smaller than the usual 150 km maximum radius to minimize uneven coverage due to shorter profiles on the landward side of the vortex.

In the analysis scheme, the in situ and radar data were renavigated into a coordinate system moving

along an objectively constructed cyclone track (Willoughby and Chelmow 1982), and composites of radar reflectivity were prepared as Marks (1985) describes. Although the objective cyclone track generally described the vortex motion during a series of flights and the radar composites represented part of one flight, analysis of the in situ observations dealt with single, complete flights as units or, rarely, with two or three flights when the cyclone was evolving slowly.

The data processing for in situ observations was an elaboration of the method used in previous studies (Willoughby et al. 1982, 1984). At each radius, the temporal variations of the swirling wind, V, and isobaric height, Z, were approximated as time mean values ($\bar{V}$ and $\bar{Z}$, the intercepts) and rates of linear change with time (α_V and α_Z, the slopes) for the interval during which the observations were taken:

$$\left.\begin{aligned} V(r,t) &\approx \bar{V}(r) + \alpha_V(r)(t-\bar{t}) \\ Z(r,t) &\approx \bar{Z}(r) + \alpha_Z(r)(t-\bar{t}) \end{aligned}\right\}. \qquad (1)$$

In (1), $\bar{t}$ is the average of the times of observation, t_i ($i = 1, 2, 3 \cdots N$). The analysis scheme used sums of overlapping B-splines (Ooyama 1987) to construct the radial variation of the intercepts and slopes. The intercepts derived from a least-squares fit of the splines to the observations (V_i or Z_i, $i = 1, 2, 3 \cdots N$) as functions of radius regardless of t_i or direction from the center. The slopes derived from a fit of the splines, weighted by $(t_i - \bar{t})^2$, to $(V_i - \bar{V})$ or $(Z_i - \bar{V})$, weighted by $(t_i - \bar{t})$. Thus, $\bar{V}$ and $\bar{Z}$ represented statistical estimates of the swirling wind or isobaric height at time $\bar{t}$. Evaluation of (1) at t_1, the time of the first observation, or at t_N, the time of the last observation, estimated radial structure when the aircraft arrived or when it departed. Because the spline algorithm had inherent spatial smoothing that enhanced persistent features relative to random fluctuations, it was more sensitive to moving wind maxima than the earlier algorithm based upon sorting the data into radial bins and calculating the slope and intercept for each bin independently.

Figure 2a illustrates application of this analysis to calculate the time mean value and 6 h change of the swirling wind in Hurricane Danny during the 20.333 h interval between 1505 UTC 14 August and 1125 UTC 15 August 1985. Here $\bar{V}$ is an estimate of the wind as a function of radius at $\bar{t}$, 0115 UTC 15 August; $\alpha_V \times$ (6 h) is the change expected over a 6 h interval, equivalent to 6/20.333 of the actual total change. Normalization of the change to a 6 h interval facilitates comparison among cases. Figure 2b is an alternate presentation of the same data. It shows the swirling wind, $\bar{V} \pm \alpha_V \times$ (10.167 h)—that is, at 1505 UTC 14 August and at 1125 UTC 15 August—and the normalized change. Detailed discussion of Danny's track and development follows in section 3.

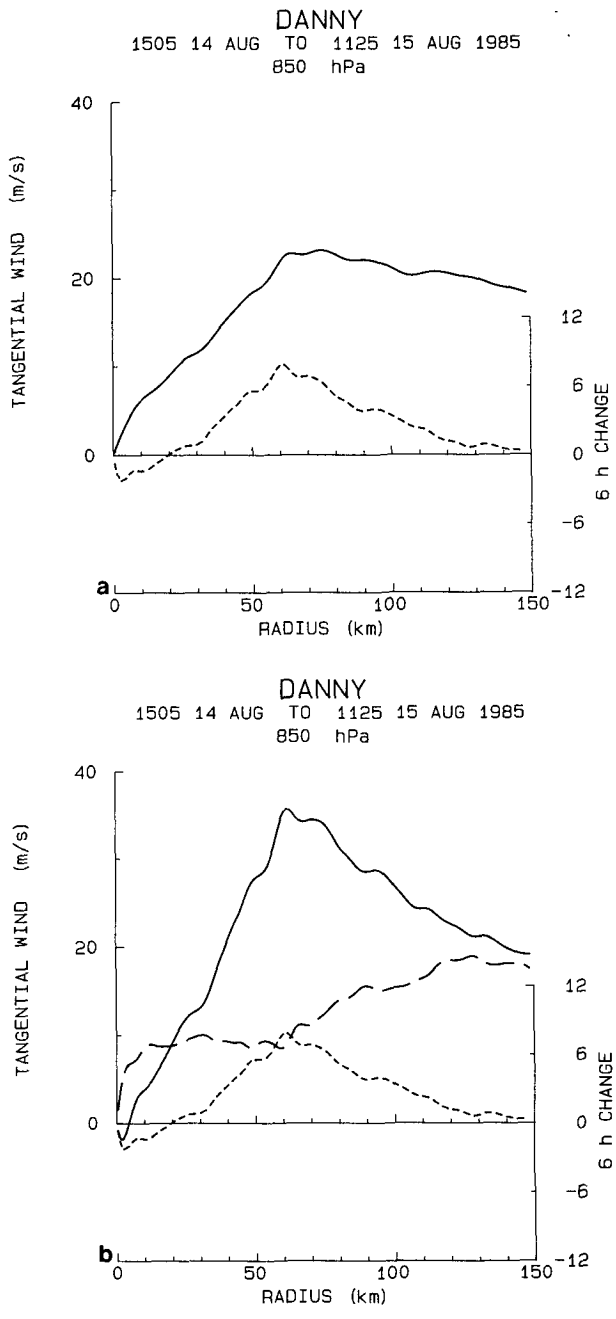

FIG. 2. The development of Hurricane Danny's primary circulation during flights 850814I and 850815H. (a) The solid curve shows the time mean axisymmetric swirling wind, and the short-dashed curve is the wind's change in 6 h. (b) The same data represented in terms of the total change; the long-dashed curve shows the axisymmetric swirling wind at the start of 850814I, and the solid curve shows the swirling wind at the end of 850815H. The short-dashed curve is the same as in Fig. 2a.

3. Development of an ordinary hurricane

Hurricane Danny of 1985 exemplifies development of a single convective ring. Danny formed from an African wave that traversed the Atlantic and the Ca-

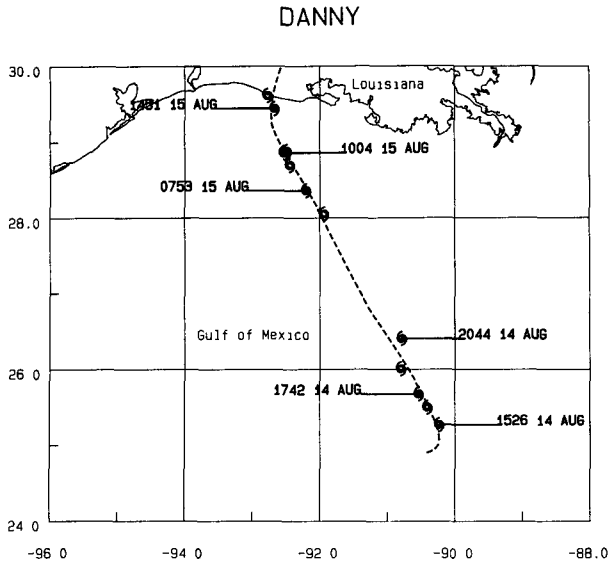

FIG. 3. Track of Hurricane Danny during flights 850814I, 850815H, and 850815I.

ribbean. The wave became a tropical depression just before it crossed western Cuba into the Gulf of Mexico. In the Gulf, the depression intensified quickly, reaching hurricane intensity on 14 August, making landfall on the Louisiana coast the next day (Case 1986).

Research aircraft monitored Danny for >27 h as the cyclone tracked northwestward toward landfall (Fig. 3). Figure 2 shows the evolution of Danny's primary circulation for 20.333 h when the data coverage, as defined in Fig. 1, was good. After 1125 UTC 15 August, Danny had approached the coast so closely that aircraft could not enter the northern semicircle and the coverage deteriorated to poor.

At 1505 UTC 14 August, Danny's strongest winds lay nearly 130 km from the center and the convection was poorly organized. As time passed, the wind on the inward side of the maximum increased, causing the RMW to contract to 60 km radius and V_{max} to increase from 18 to 36 m s^{-1}. The Rossby number, Ro, evaluated at the RMW increased from 2 to 8, where Ro $= V/fr$, f is the Coriolis parameter, and r is the radius. The locus of convection contracted to keep pace with the RMW and the area within the eye cleared. Figure 4 shows that the eyewall was a collection of individual convective cells rather than a locus of uniform mesoscale ascent. A companion paper (Willoughby 1990) demonstrates that the swirling wind was in gradient balance with the isobaric height. It further shows that the isobaric height fell most rapidly inside the RMW, producing a radial height-fall gradient that sustained the wind's increase. Thus, both the swirling wind and its change obeyed the gradient wind relation.

Hurricanes Juan of 1985 and Charley of 1986 exhibited large eyes and gradual intensification similar to Danny's. All three developed according to the con-

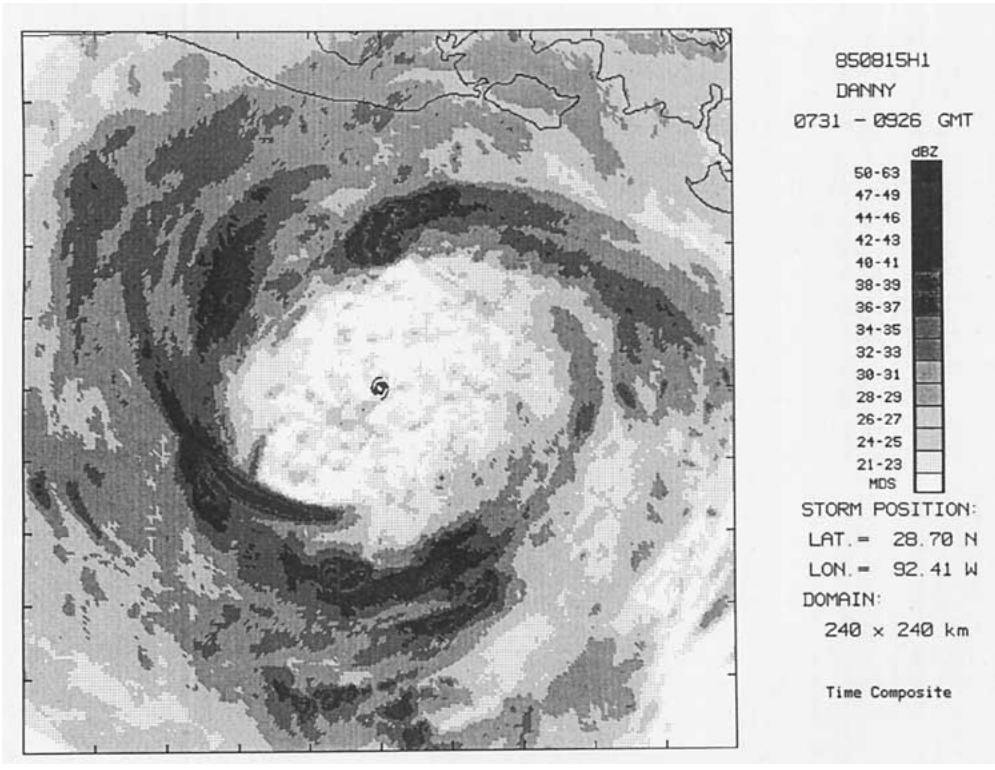

FIG. 4. Composite radar reflectivity in Hurricane Danny at the middle of flight 850815H. North is at the top.

vective ring model. They differed from Anita, David, and Allen in that their RMWs were larger, their Rossby numbers—though still >1—were smaller, and only a single ring formed in each case. They confirm the model clearly in other aspects: localization of the height falls within the RMW, gradient balance, localization of the convection near the RMW, and contraction of the RMW. To show a range of contrast with these ordinary hurricanes, section 4 examines tropical storms that generally did not exhibit convective rings, and section 5 illustrates the more complicated role that convective rings play in major hurricanes.

4. Nondevelopment

Tropical Storms Arthur of 1984 and Isabel of 1985 illustrate nondeveloping tropical cyclones. Neither formed a persistent convective ring; instead convection occurred in isolated outbursts that perturbed the vortex, but could not sustain intensification.

Arthur formed from an African wave east of Trinidad (Lawrence and Clark 1985). Its circulation persisted from 28 August until 5 September. Research aircraft flew a single sortie each day from 31 August through 2 September as Arthur tracked northwestward parallel to the Lesser Antilles (Fig. 5). The data comprise 22 radial profiles, giving good coverage over a storm-centered domain 250 km in radius. Because the aircraft observed few profiles over a large domain, the data were analyzed as overlapping pairs of flights: 840831H combined with 840901H and 840901H combined with 840902H. Figure 6a shows the radial variation of the swirling wind as typical values decreased from 10 to 8 m s^{-1} on 31 August and 1 September. The wind profile was nearly flat from 70 to 250 km radius, over which interval Ro varied from 3.5 to 1, based upon a swirling wind of 10 m s^{-1} at 16°N.

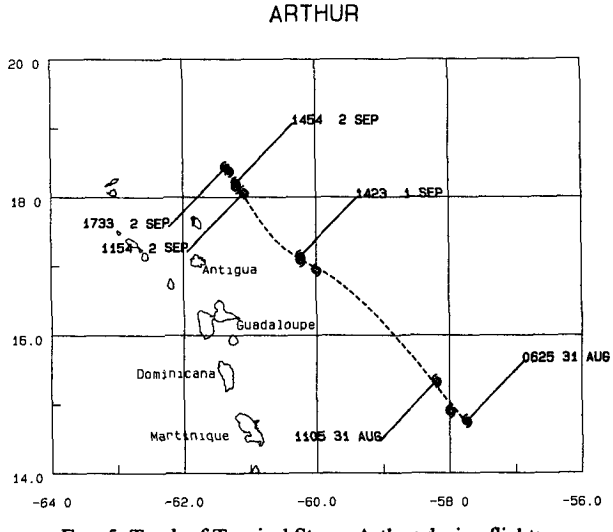

FIG. 5. Track of Tropical Storm Arthur during flights 840831H, 840901H, and 840902H.

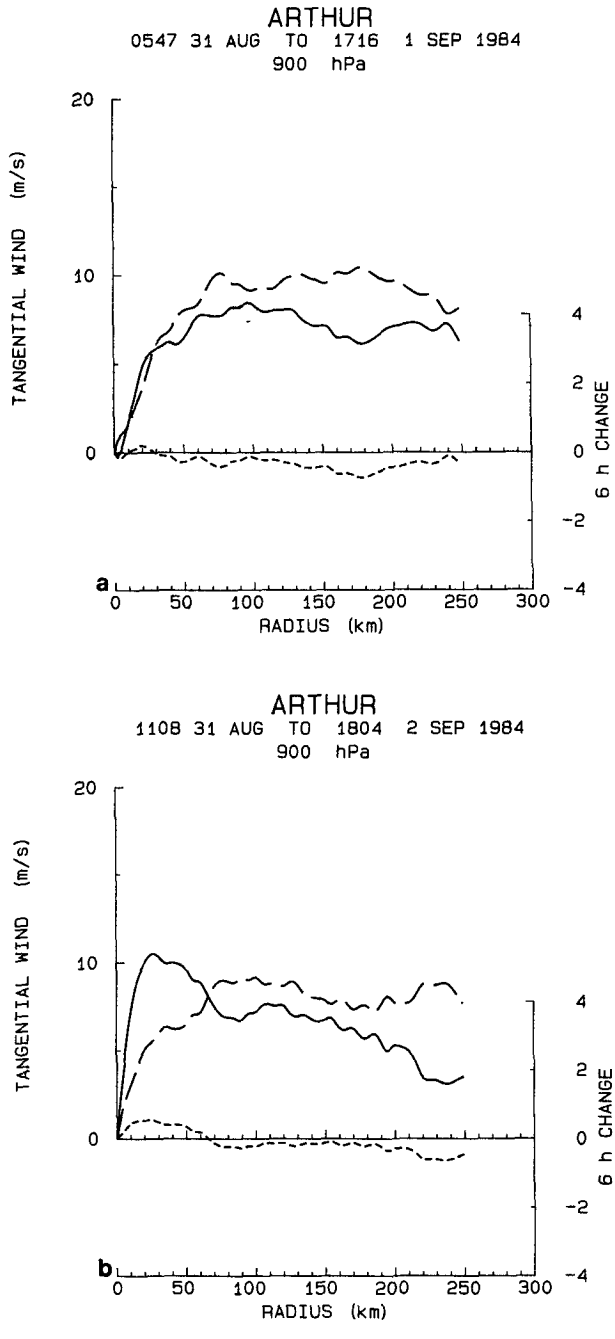

FIG. 6. Development of Arthur's primary circulation during (a) flights 840831H and 840901H, and (b) flights 840901H and 840902H. The curves have the same meaning as in Fig. 2b.

On 1 September, the convection was concentrated in the northeast corner of the domain with a few cells scattered widely near the center (Fig. 7a). The arrangement of cells hints at circular organization, but it has none of the aspect of a vigorous tropical cyclone. On the previous day, 31 August (not shown), more convection lay in the northeast corner and less near the center.

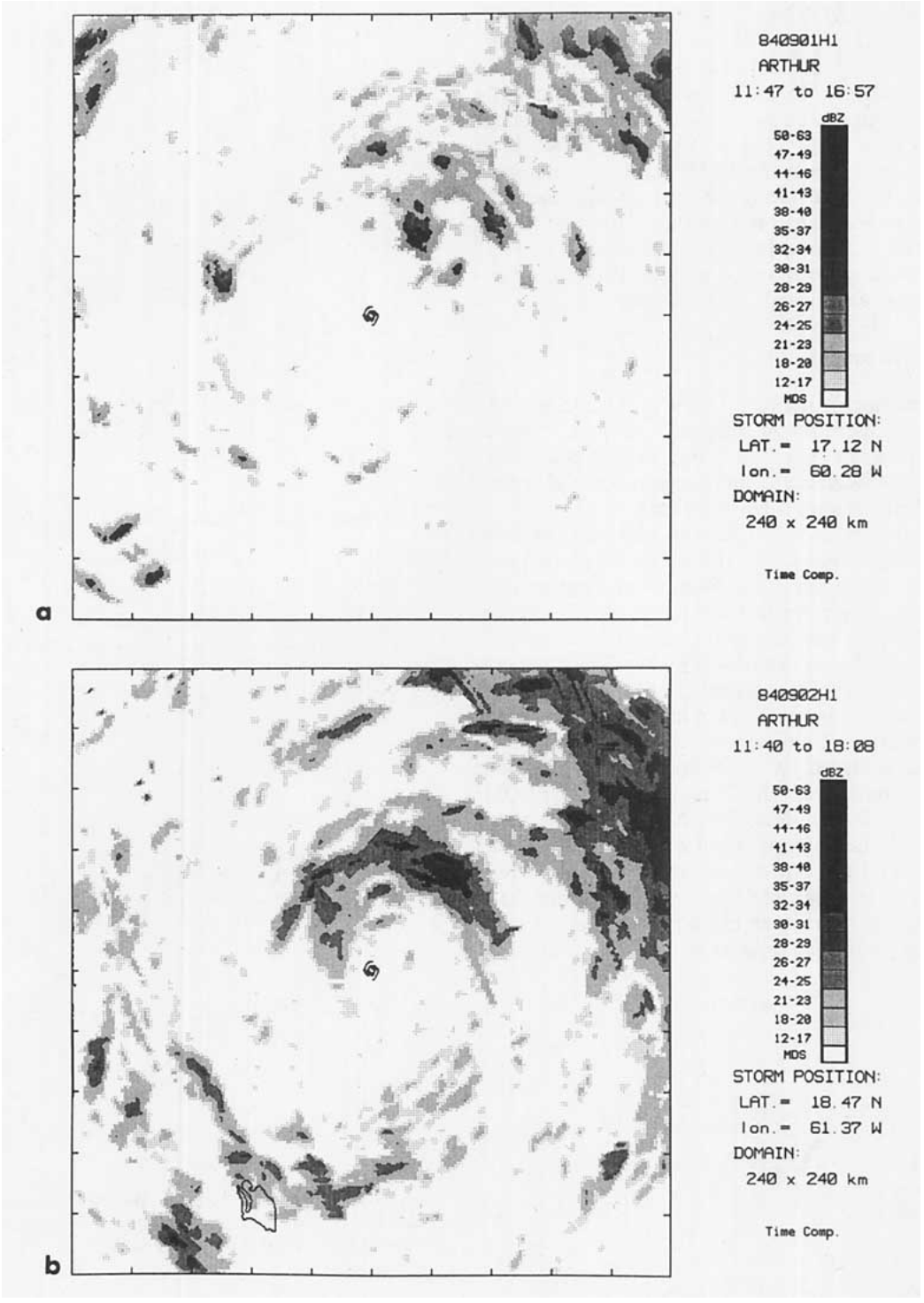

On 2 September, the convection moved closer to the circulation center and its organization became a bit more like a developing tropical cyclone (Fig. 7b). Although the vortex continued to weaken beyond 70 km, inside that radius it strengthened, forming a well defined RMW 30 km from the center with V_{max} = 11 m s^{-1} (Fig. 6b). This intensification was relative: the rate of wind increase was 10% of that in Danny, and a typical radar reflectivity was 30 dBZ, equivalent to a rain rate of 2.5 mm h^{-1} [using Jorgensen and Willis' (1982) Z–R relationship] compared with 40 dBZ and 13 mm h^{-1} in Danny. Moreover, the intensification

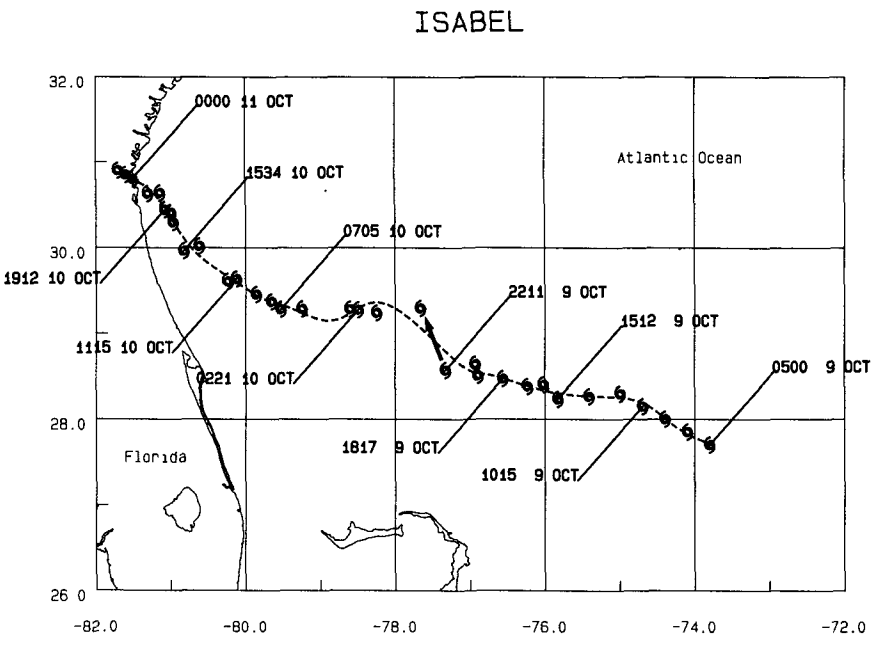

FIG. 8. Track of Tropical Storm Isabel during flights 851009I, 851009H, 851010I, and 851010H. The arrow indicates the convectively induced track displacement.

was an interruption, not a reversal, of a general weakening; satellite imagery showed that Arthur dissipated over the next 3 days, probably because it encountered vertically sheared environmental flow and the weak vortex could not extract enough latent heat from the sea to maintain convection.

Although the cyclone-relative wind defined a closed circulation, Arthur was an open wave in the earth-relative winds. An axis of calm extended southwest of the center normal to the track where the vortex translation and swirling wind opposed each other. If the vortex had been weaker, it would not have been possible to find the center from aircraft in real time. Nevertheless, Ro near the center was always >1 and reached a value of 8 during the "intensification" on 2 September. Thus, Arthur was a nonlinear vortex in the sense that the relative acceleration (V^2/r) was greater than the Coriolis acceleration (fV). On 2 September, the wind maximum formed and contracted in response to convective heating, much as happens in a convective ring, but active convection did not persist long enough to prevent Arthur's dissipation.

Tropical Storm Isabel formed in an area of disturbed weather that separated from an African wave in the Caribbean. It progressed northward in the Atlantic and finally turned westward to landfall and dissipation on the southeastern U.S. coast (Case 1986). During the 43 h before landfall when research aircraft monitored Isabel (Fig. 8), strong upper tropospheric southwesterly flow led to suppressed convection and slowed Isabel's westward track. At the start of this period, the primary circulation was about twice as strong as Arthur's (Fig. 9), but Isabel weakened consistently, becoming a tropical depression by landfall.

As in Arthur, the wind profile was flat. During the time shown in Fig. 9, intense convection erupted north of the center. The cell, shown as a radar image in Fig. 10, deflected Isabel's center to 40 km north of the

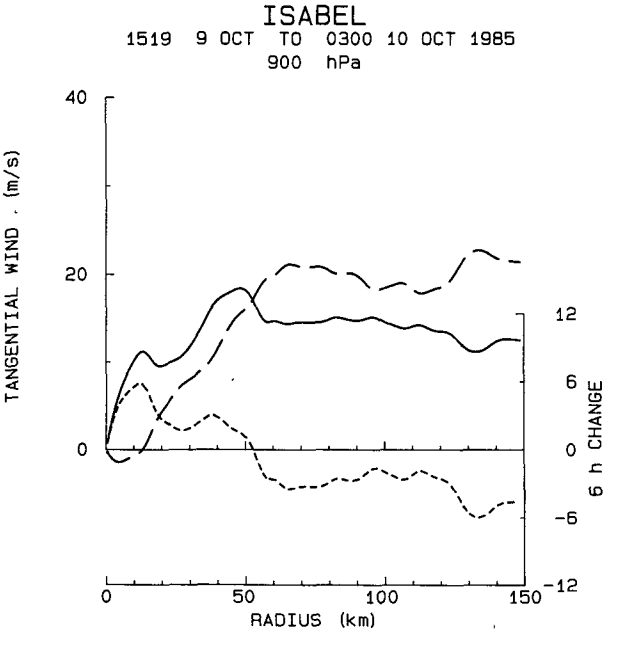

FIG. 9. Development of Isabel's primary circulation during flights 851009I and 851009H. The curves have the same meaning as in Fig. 2b.

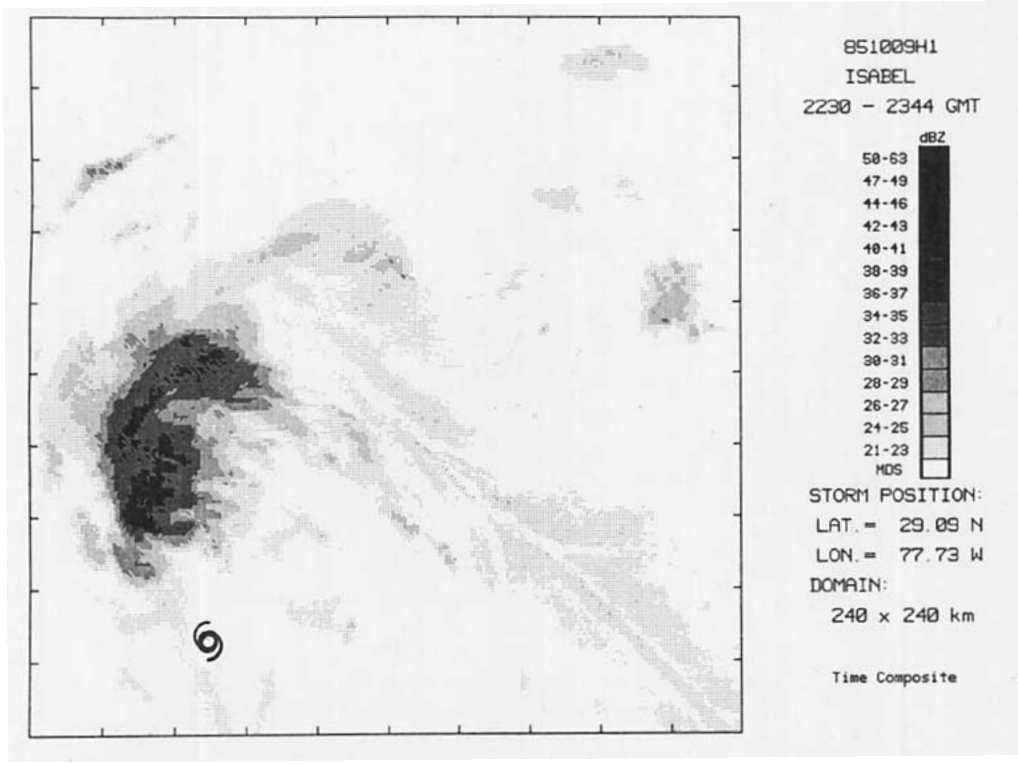

FIG. 10. Radar reflectivity composite of Isabel during flight 851009I. The circulation center is placed near the southwestern corner of the frame to show the cumulonimbus north and northeast of the center.

former track. Similar convectively induced track perturbations have been documented previously (Neuman and Boyd 1962; Willoughby and Chelmow 1982). Much as happened in Arthur, the wind near the center strengthened briefly, but the long-term weakening trend continued after the cell dissipated. Indeed, the flat wind profile with episodic cellular convection interrupting long-term weakening seems to characterize nonde-

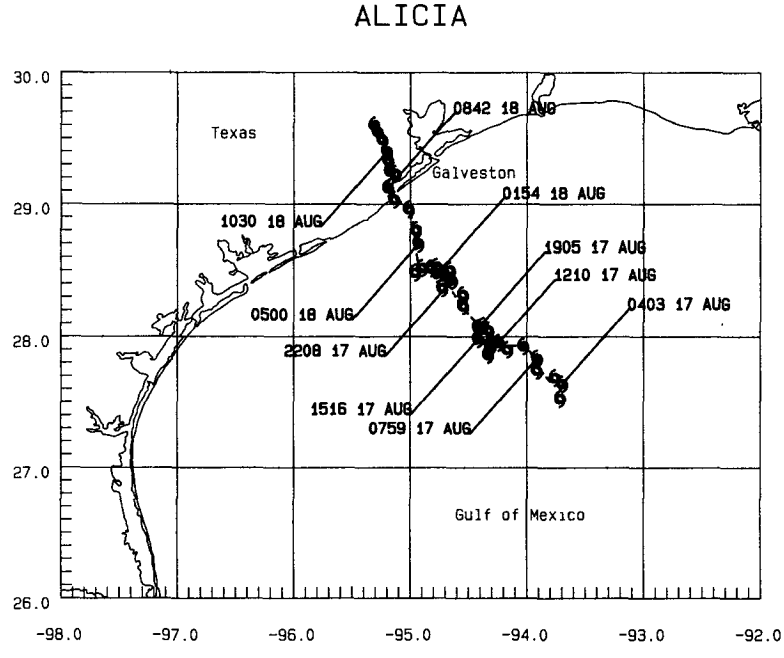

FIG. 11. The track of Hurricane Alicia during flights 830817I, 830817H, 830817I2, and 830818H.

veloping tropical cyclones, in contrast with the persistent convective rings of intensifying ones.

5. Development of major hurricanes

This section describes the detailed development of four major hurricanes: Alicia of 1983, Diana of 1984, Elena of 1985 and Gloria of 1985. Research aircraft monitored the first three hurricanes almost continuously from formation to landfall and, despite interruptions, managed to observe the essential features of Gloria's development as well. These observations, combined with less detailed discussion of two major hurricanes since 1986, provide substantial confirmation and extension of the convective ring hypothesis.

Hurricane Alicia formed on a stagnating frontal trough in the northwestern Gulf of Mexico and followed an irregular northwestward track (Fig. 11) to landfall on the Texas coast near the western end of Galveston Island (Case and Gerrish 1984). Figure 1 shows the changing distribution of radial passes during the research flights in Alicia. A subset of these passes, all oriented along a northeast–southwest axis parallel to the shoreline (Fig. 12), illustrates development of the vortex. At 0759 UTC 17 August the eye was 40–50 km in radius with V_{max} = 35 m s^{-1}. At 1300 UTC the outer eyewall formed 100 km from the center. Between then and 0000 UTC on the 18th both eyewalls contracted, attaining nearly equal V_{max} = 45 m s^{-1}. Subsequently, the outer eyewall continued to contract and became asymmetric, retaining its intensity on the east side but weakening on the west where the wind

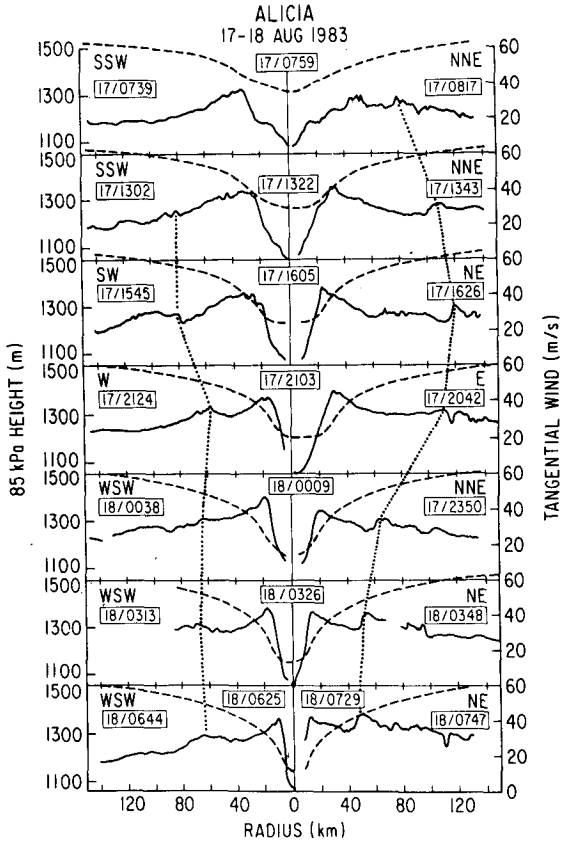

FIG. 12. Radial profiles of the swirling wind (solid curves) and 85 kPa height (dashed curves) along an axis parallel to the coast in Alicia. The dotted lines connect positions of the outer wind maximum. Numbers in boxes indicate the time (UTC) the aircraft reached the cyclone center and the ends of the passes. Directions from the cyclone center also appear at the sides.

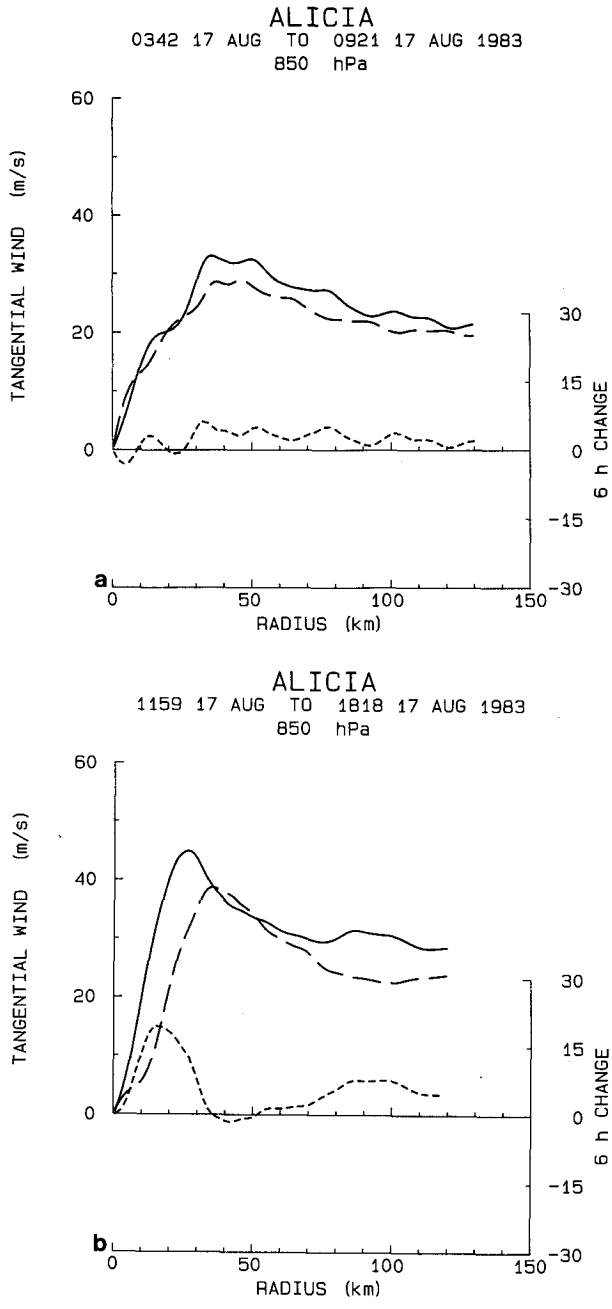

FIG. 13. Development of the primary circulation in Alicia: (a) initial intensification during flight 830817I, and (b) formation of the outer eyewall and further development of the main eyewall during flight 830817H. The curves have the same meaning as in Fig. 2b.

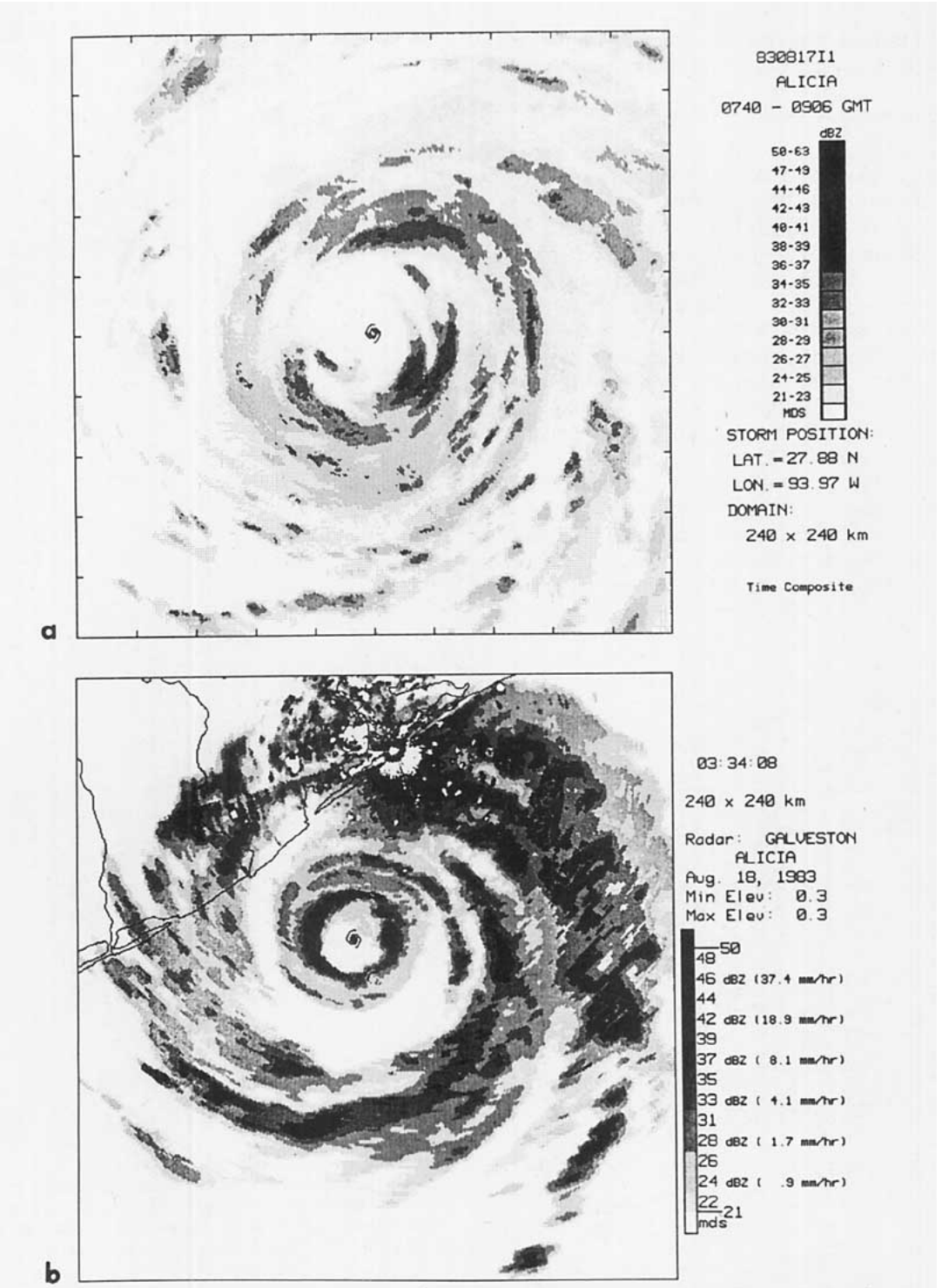

FIG. 14. Radar reflectivity in Alicia: (a) composite of aircraft radar during flight 830817I, showing loosely organized convection; (b) a single sweep from the Galveston WSR-57 radar, showing a well-formed outer eyewall surrounding the original eyewall and joining the principal band, which extends north through southeast outward from the outer eyewall.

blew offshore. The inner eyewall remained more symmetric but weakened to $V_{max} < 40$ m s^{-1} before landfall at 1000 UTC on the 18th. Color isotach analyses depicting the foregoing evolution accompany Willoughby et al. (1985).

Statistical estimates of the axisymmetric primary circulation are consistent with the individual profiles. They show that early during flight 880917I1 as Alicia reached hurricane intensity, increasing swirling wind (Fig. 13a) and convection (Fig. 14a) spread over a wide

radial interval. Later during flight 830817H, the wind increases became more localized inside the eyewall and at an emerging outer wind maximum (Fig. 13b). This pattern of development continued during flight 830817I2 (not shown). Between 0342 and 1757 UTC, Ro at the RMW increased from 10 to 23. On radar, the original eyewall, and later the outer eyewall, formed from convective cells that detached from the inward edge of the principal band (as defined by Willoughby et al. 1984) and coalesced into rings of convection (Fig. 14b). Throughout the time before landfall at 0842 UTC 18 August, reflectivities in both eyewalls increased as the moats between the eyewalls and between the outer eyewall and the principal band cleared and widened. The individual profiles in Fig. 12 show that Alicia reached the shore just as the outer eyewall began to encroach on the inner, but the data coverage was too poor for reliable estimation of the axisymmetric primary circulation during flight 830818H. The development of the outer eyewall just before landfall in Alicia resembled that in Anita, although Anita was more intense.

Figure 15a shows Hurricane Diana's track while research aircraft carried out intensive monitoring. Diana formed on a trailing frontal trough east of the central Florida coast on 8 September 1984. After formation, Diana tracked northward then northeastward, finally approaching the coast near Wilmington, North Carolina, on 12 September. Diana then spent the next 25 h in an anticyclonic loop east of Wilmington (Fig. 15b) before making landfall south of the city at 0700 UTC 13 September. Over land, Diana resumed northeastward motion and recurved into the North Atlantic (Lawrence and Clark 1985). The data coverage was good when Diana was far at sea, becoming fair during both approaches to the coast, and then poor at landfall.

Diana's early intensification was slow. Between 1400 UTC 9 September and 0000 UTC 10 September, intense convection erupted on the western side of the vortex (Fig. 16a) and moved to the south side, deflecting the cyclone's track > 50 km westward and stopping its northward progress for nearly 5 h (Fig. 16b). Similar convectively induced track perturbations occurred in Tropical Storm Isabel (section 4) and in Hurricane Charley of 1986. As in Arthur, Isabel, and Charley, the convective eruption preceded an interval of quiescence. Figures 17a and 18a, respectively, show the primary circulation's development and the radar reflectivity distribution during this time. During the 17 h after the eruption, Diana intensified no more rapidly than a nondeveloping tropical storm. Although the radar showed an orderly pattern of spiral bands, reflectivities were low: 30 dBZ, equivalent to 2.5 mm h^{-1} of rainfall.

Early on 11 September, intensification resumed. Figure 17b shows that Diana's primary circulation developed according to the classic pattern for a single convective ring in an intense tropical cyclone: the wind increased most rapidly at and inside the wind maximum so that the RMW contracted as V_{max} increased. Between the earliest and latest times in Fig. 17, Ro at the RMW increased from 15 to 31. This phase of Diana's intensification was virtually identical to Hurricane Allen on 8 August 1980 (Willoughby et al. 1982).

By midday on the 11th, an outer wind maximum formed (Fig. 19a) when two spiral bands wrapped around the center to form an outer eyewall (Fig. 18b). The inner eyewall continued to strengthen as the outer

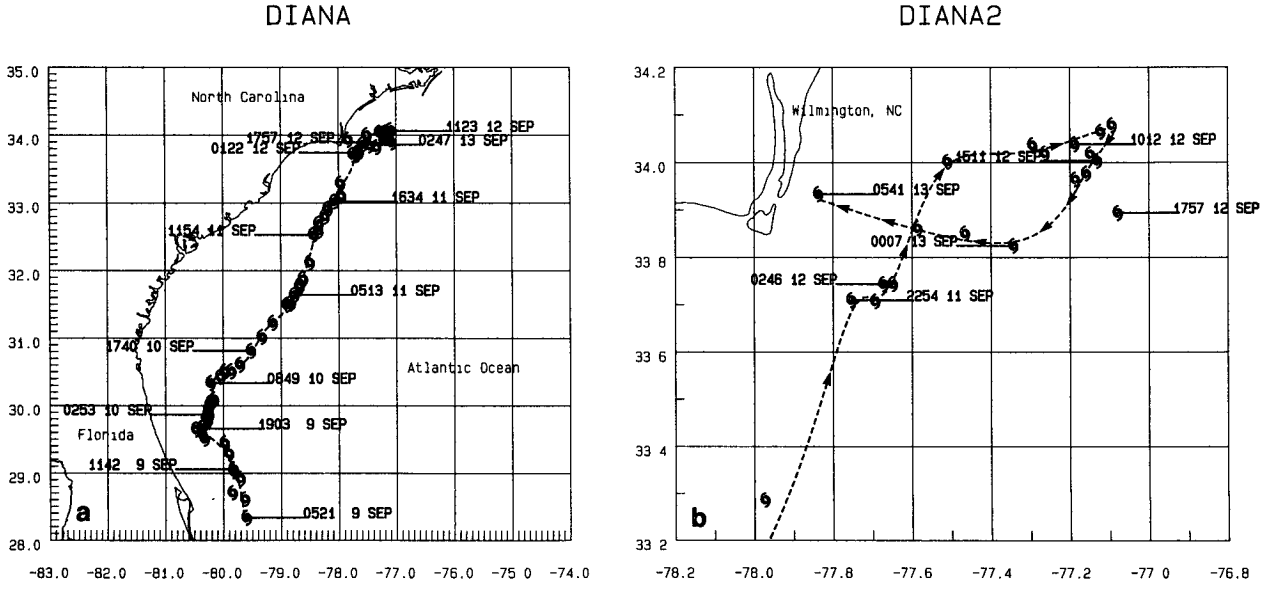

FIG. 15. (a) Track of Hurricane Diana for between 9 and 13 September 1984, and (b) detail showing the anticyclonic loop on 12–13 September.

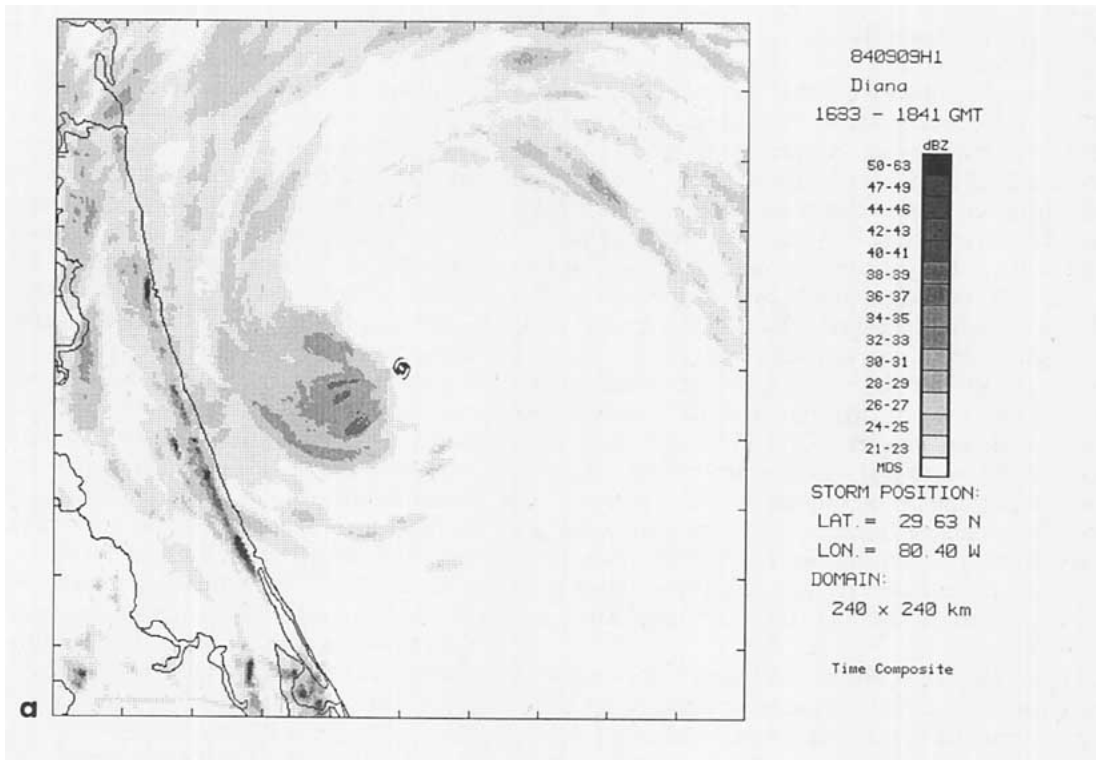

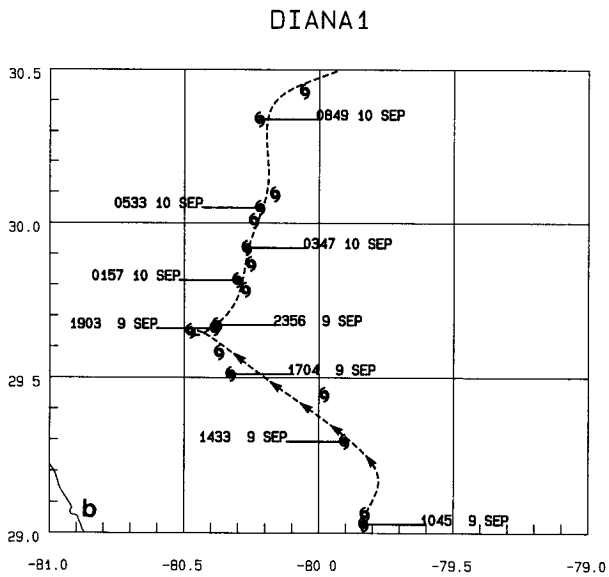

FIG. 16. (a) Radar reflectivity composite showing the convective outbreak west and south of Diana's center on 9 September 1984. (b) Detail of Diana's track on 9 and 10 September. The arrowheads indicate the convectively induced displacement.

eyewall developed. At 0306 UTC 12 September, V_{max} reached its largest value, 60 m s^{-1}, corresponding to Ro = 39. As Diana made its first approach to shore, the outer eyewall's development faltered because its northwest quadrant passed onshore. The inner eyewall also weakened, probably because of the combined influence of nearby land and the outer eyewall (Fig. 19b). During the morning of 12 September as Diana tracked eastward offshore at the start of its anticyclonic loop, the outer eyewall intensified again, but the inner eyewall continued to abate (Fig. 19c). During this interval, Diana's appearance on radar showed two pronounced concentric eyewalls and a well-defined principal band east of the center (Fig. 18c). This radar composite is almost identical with Hurricane David on 30 September 1979 (Willoughby et al. 1982). As Diana reversed course toward the west and eventual landfall, the outer wind maximum replaced the inner (Fig. 19d), leaving a single partial eyewall visible on radar (Fig. 18d). Just before landfall, V_{max} declined to 42 m s^{-1}, corresponding to Ro = 16. Thus, these observations confirm the hypothetical cycle based upon earlier observations.

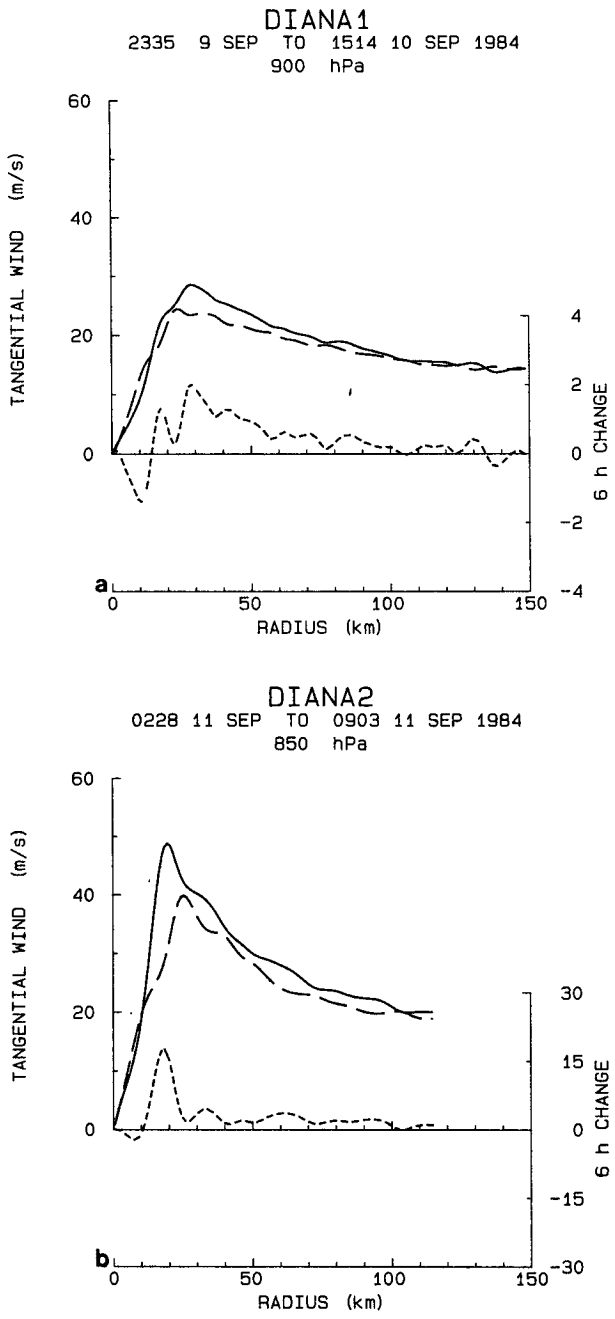

FIG. 17. Initial development of Diana: (a) early slow intensification observed during flights 840909I2 and 840910H, (b) rapid development of the original eyewall during flight 840911I. The curves have the same meaning as in Fig. 2b.

Hurricane Elena of 1985 began as a tropical wave that crossed the Atlantic and passed over Cuba into the Gulf of Mexico. Elena intensified gradually as it moved northwestward, then northeastward, in the Gulf on 29–31 August (Fig. 20a). On 31 August and 1 September, passage of a midlatitude trough induced an anticyclonic track loop (Velden 1987) that required 22 h to complete in Apalachicola Bay (Fig. 20b). Finally, Elena tracked toward the west-northwest making landfall near Biloxi, Mississippi, at 1300 UTC 2 September. Elena intensified slowly, reaching a minimum central pressure of 951 mb as it emerged from the anticyclonic loop (Case 1986). In all, Elena experienced four convective rings, denoted by I–IV. Of these, only ring III fit the model of a sharp wind maximum contracting in response to vigorous convective heating. Rings I and II were asymmetric features that never developed fully, and IV was a failed outer eyewall.

In the early stages of Elena's development, the wind profile was flat, much like that in nondeveloping tropical storms (Fig. 21a). At this stage, Ro was 6, comparable with the values in Arthur or Isabel. Superimposed upon the flat wind profile were inward propagating rings I and II. The first appeared at 150 km radius as an increase of the swirling wind and propagated to 70 km radius over an interval of 14 h on 29 and 30 August (Figs. 21a, b), causing a clearing of the vortex center (Figs. 22a, b). Ring I coincided, not with an organized ring of convection, but with a concentration of convection in the southeast quadrant of the vortex. Ring II (not illustrated) underwent a similar evolution on 31 August while Elena was in Apalachicola Bay. The convection in rings I and II remained asymmetric, but because it introduced net heating over an annular radial interval, it supported contracting maxima of the axisymmetric swirling wind, without, however, having great effect on Elena's slow intensification. Reanalysis of observations from Hurricanes Gert and Frederic with the present spline-based algorithm, which detects subtle wind maxima more sensitively than the earlier algorithm based upon radial bins, showed similar features.

The data for Elena do not show clearly whether ring III was a newly formed feature or ring II reinvigorated. As Elena emerged from the anticyclonic loop, ring III caused the RMW to contract to 25 km and V_{max} to increase to 51 m s^{-1}, making Ro = 28 at the RMW (Figs. 21c and 21d). The rate of intensification then was comparable with the other major hurricanes in this study. As occurred in other such cyclones, outer convective ring IV formed (Figs. 22c and 22d). Although on radar ring IV ring looked like outer rings in the other major hurricanes and had a wind maximum, animated displays of the Apalachicola radar showed that it appeared and vanished at intervals of a few hours. Ring IV neither replaced the original eyewall nor did it, apparently, cause Elena to weaken. The development of ring II correlated at 30 h lag with an increased upper-level eddy angular momentum influx and enhanced outflow as Elena interacted with a passing midlatitude trough (Molinari and Vollaro 1989). The end of the trough-induced angular momentum influx and proximity to land seem to be more likely explanations for Elena's slight weakening on 2 September before landfall than any influence of ring IV.

Hurricane Gloria developed from an African wave, becoming a hurricane on 21 September 1985 east of

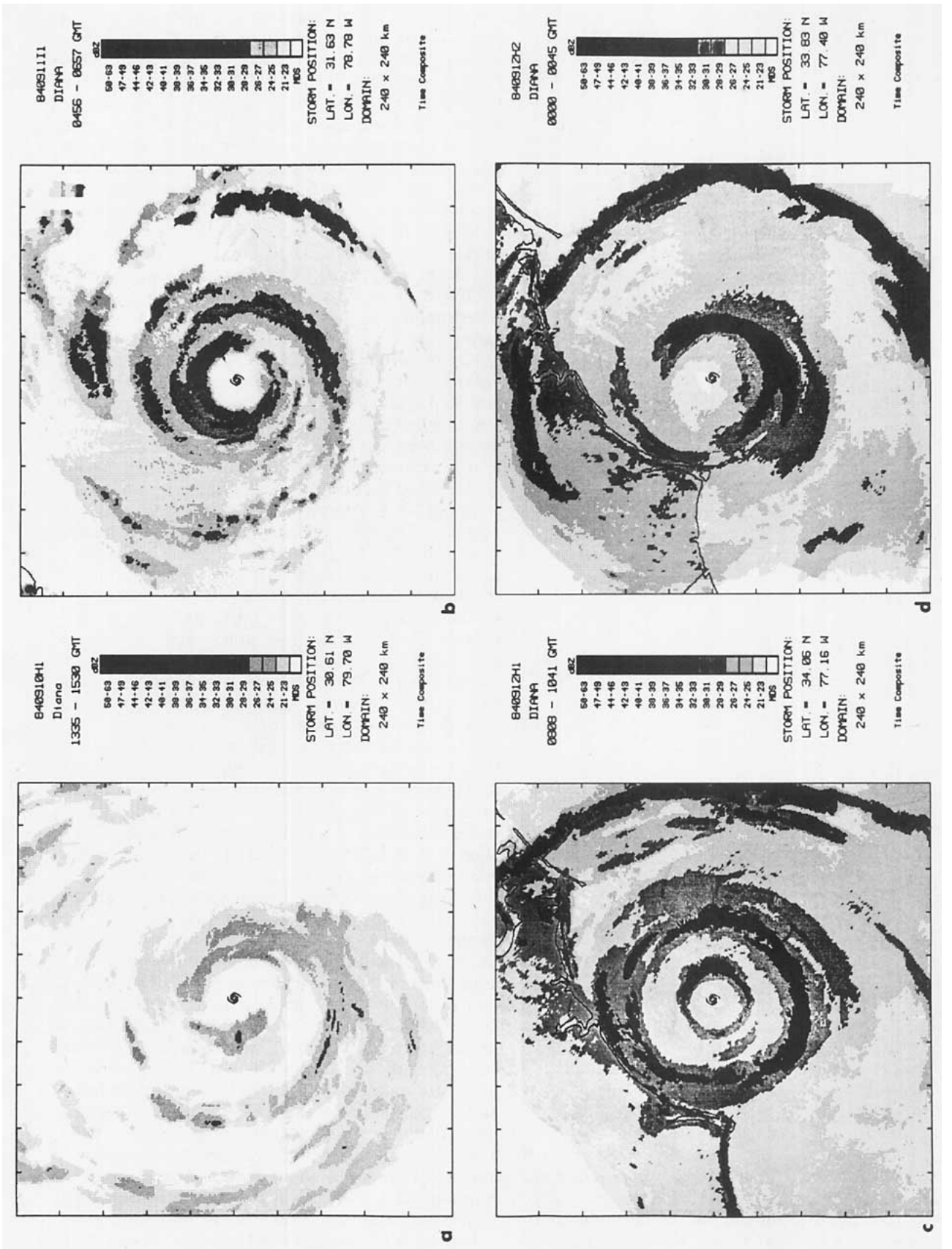

FIG. 18. Radar reflectivity composites in Diana: (a) weak reflectivities when Diana was quiescent during flight 840910H, (b) initial appearance of the outer convective ring during flight 84091111, (c) fully developed concentric eyewalls during flight 840912H, and (d) the single remaining eyewall during flight 840912H2.

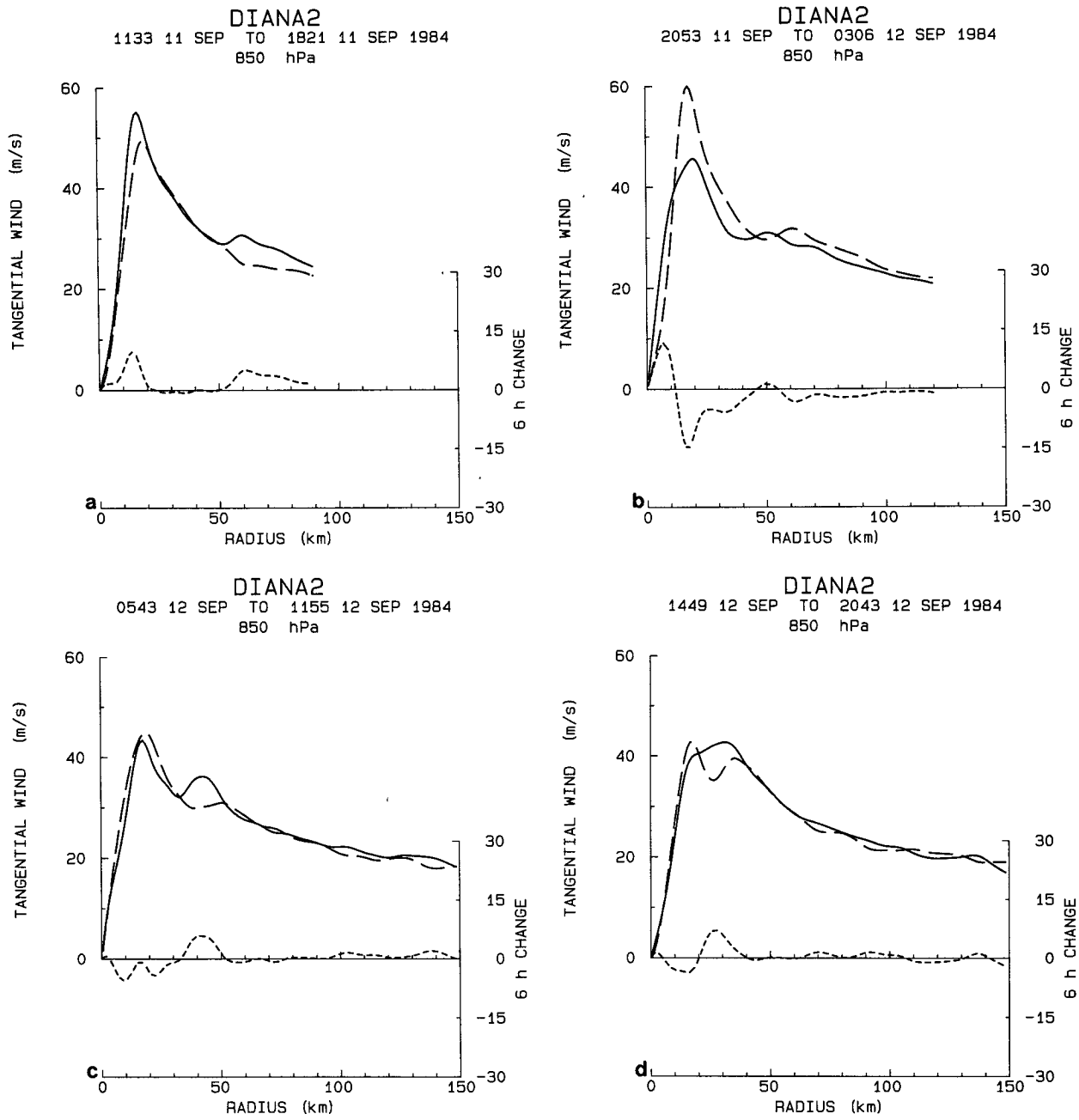

FIG. 19. Swirling wind during Diana's concentric eye cycle: (a) formation of the outer eyewall during flight 840911H, (b) faltering of both convective rings as Diana approached the coast during flight 840911I2, (c) renewed intensification of the outer ring and continued weakening of the inner as Diana moved offshore during flight 840912H, and (d) replacement of the inner ring by the outer as Diana approached landfall during flight 840912I. The curves have the same meaning as in Fig. 2b.

Puerto Rico and reaching 919 mb minimum central pressure—a record for the Atlantic—on 25 September. Gloria weakened while still on the warm water side of the Gulf Stream and tracked northward parallel to the east coast of the United States (Fig. 23), passing onshore near Cape Hatteras, then back out to sea on its way to final landfall on western Long Island (Case 1986). For a variety of reasons, the research aircraft did not begin the continuous monitoring necessary for the present analysis method until 26 September, a day after Gloria had passed maximum intensity. They did, however, obtain six traverses of the center near the time of maximum intensity: one traverse—a penetration and an exit of the eye—by the first aircraft flying

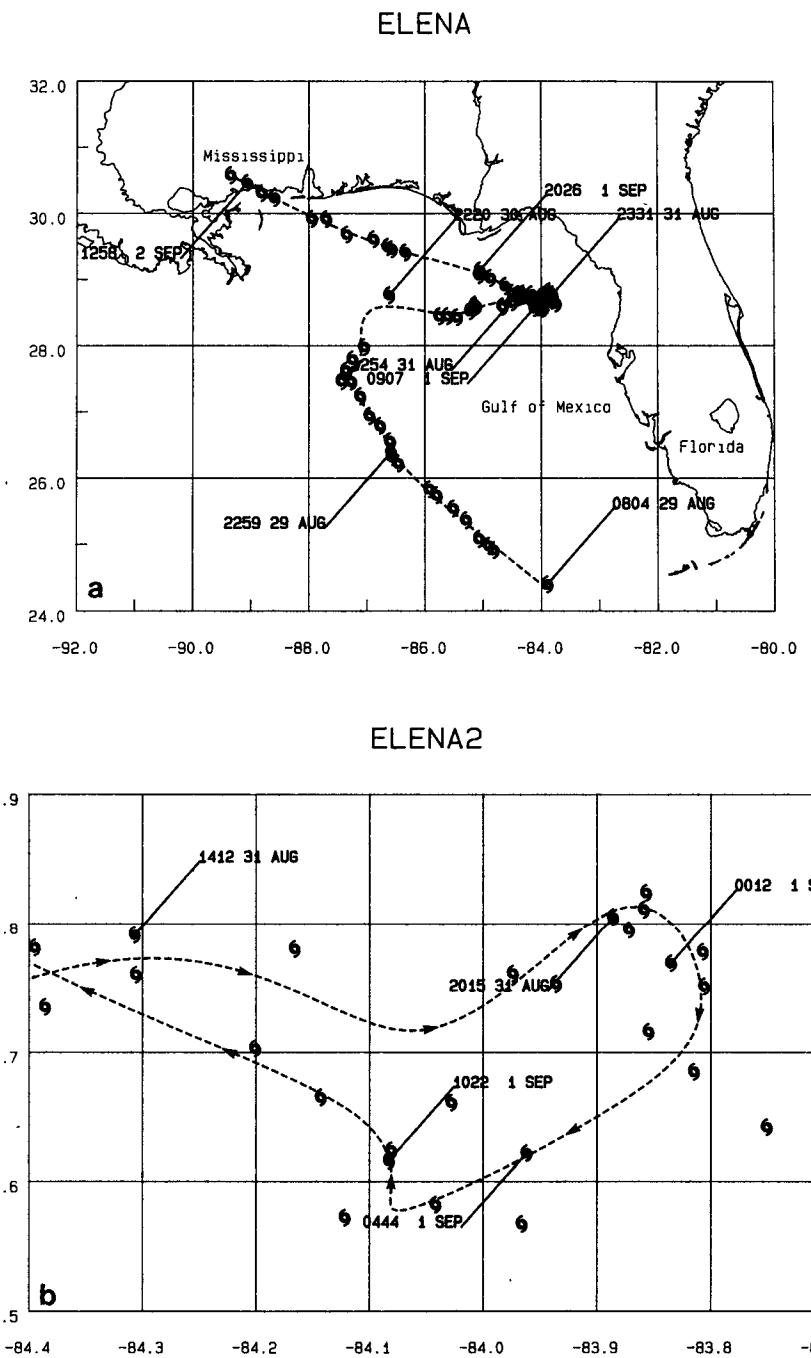

FIG. 20. (a) Track of Hurricane Elena while research aircraft monitored its development from 29 August through 2 September 1985, and (b) detail showing the anticyclonic loop on 31 August and 1 September.

at 500 hPa and a complete figure-four pattern—two penetrations and two exits—by the second aircraft at 400 hPa. Because the in situ observations were at different altitudes and spanned a relatively short time, they supported determination of only the mean wind profile, not the temporal change; but radar showed clearly that the eye diameter shrank by 8 km during this interval (Franklin et al. 1988). The mean profile at 400 hPa, shown in Fig. 24a, provides clear evidence of an inner wind maximum at 20 km radius and an outer maximum beyond 100 km. The corresponding radar composite (Fig. 25a) supports this interpretation;

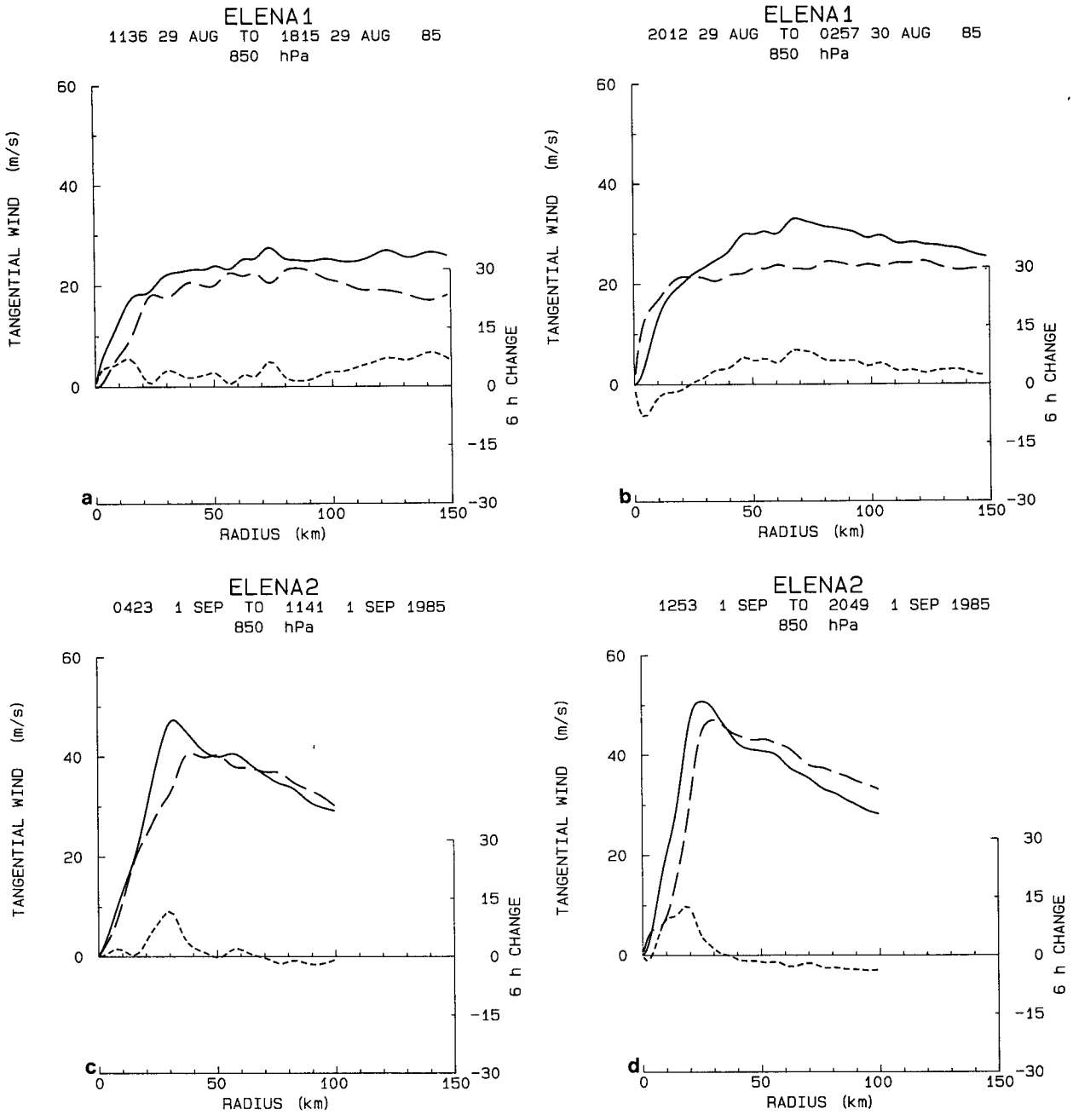

FIG. 21. Development of the primary circulation in Elena: (a) flat initial profile with the wind maximum associated with convective "ring" I (see text) appearing at 150 km radius during flight 850829I, (b) profile after maximum I had propagated inward to 70 km radius during flight 850829H, (c) intensification of the inner eyewall (convective ring III) and formation of the outer convective ring (IV) during flight 850901H, and (d) continued intensification of the ring III and quiescence of ring IV during flight 850901I. The curves have the same meaning as in Fig. 2b.

it shows an inner eyewall surrounded by a clear moat, which is, in turn, surrounded by an outer eyewall. It thus appears that Gloria had a concentric eyewall just before it weakened. In fact, examination of the wind profile at 500 hPa (not shown) indicates that a third concentric eyewall may have been present as well.

Over the next day and a half, Gloria's wind profile changed dramatically. It became flat, with 40 m s^{-1} wind extending >150 km from the center (Fig. 24b). While Gloria was well at sea and the aircraft were able to obtain good data coverage, radar showed an open inner eyewall surrounded by a partial ring of convection (Fig. 25b). The outer ring, which was clearly a different feature from the one observed on 24–25 September,

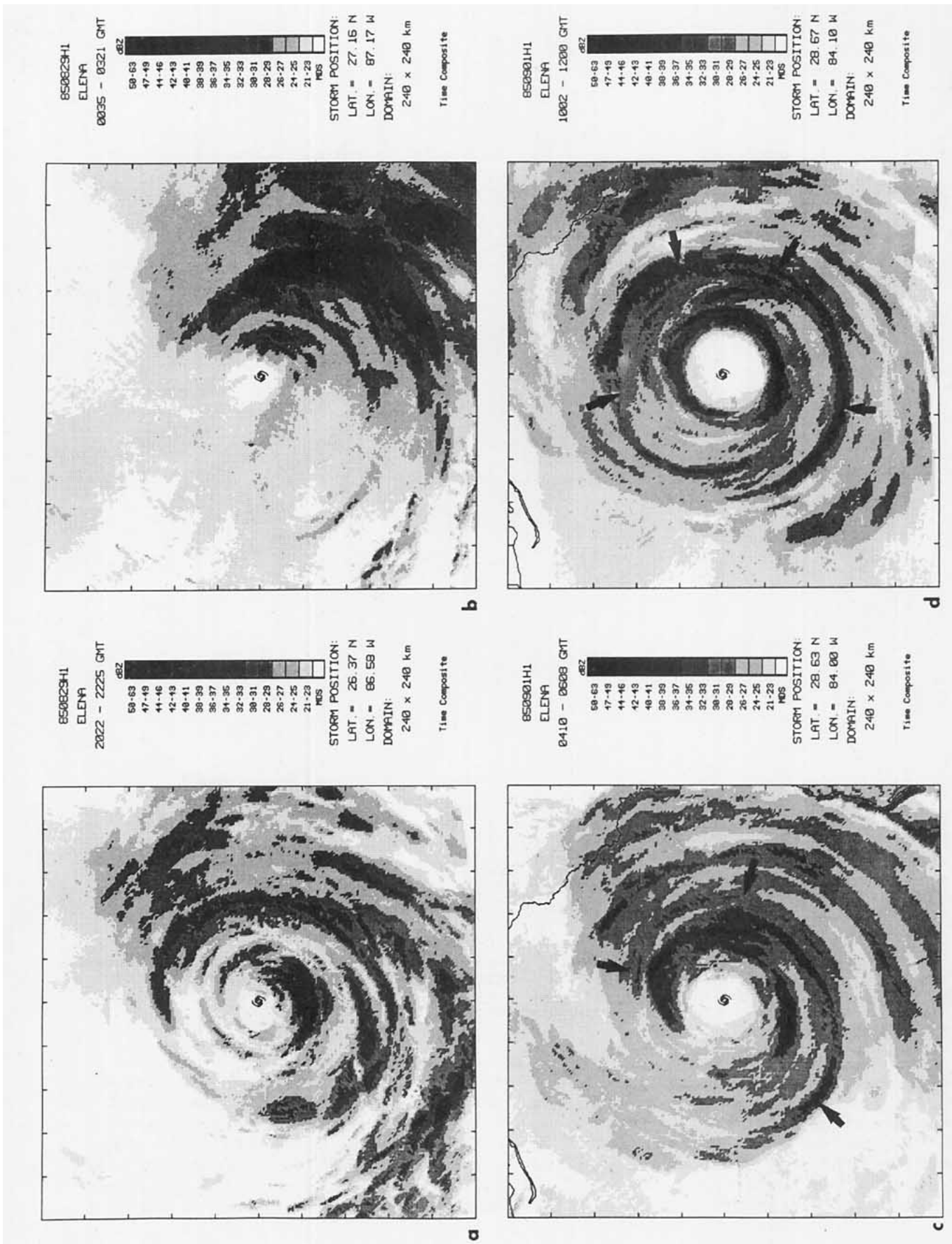

FIG. 22. Aircraft radar composites in Elena: (a) abundant radar returns near the center during flight 850829H, (b) clearing of the center later in the same flight as convection to the southeast moved inward with the wind maximum I, (c) formation of convective ring IV around ring III during flight 850901H, and (d) transient concentric eyewall later in the same flight. Arrows indicate ring IV in (c) and (d).

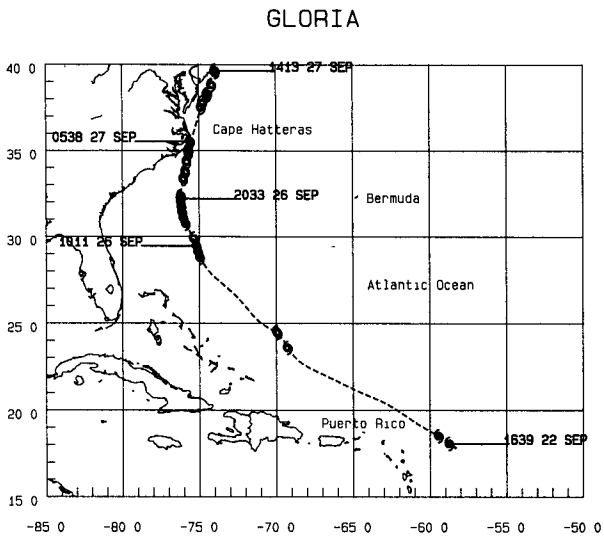

FIG. 23. The entire track of Hurricane Gloria. Detailed aircraft monitoring took place on 24–25 and 26–27 September 1985.

coincided with a wind maximum and propagated inward slowly. The clouds along its inner side of the outer ring looked like an eyewall visually from the aircraft. As Gloria approached the coast, this ring's western side passed onshore and it began to weaken. At this stage, Gloria resembled Hurricane Allen on 9 August 1980, although both convection and the wind maxima were weaker.

These hurricanes occurred during the 1983 through 1985 seasons; 1986 produced no major hurricanes; 1987 and 1988 produced one major hurricane each: Emily in 1987 and Gilbert in 1988.

Emily developed a small eye with $V_{max} = 57$ m s^{-1} south of Hispaniola on 22 September 1987 and weakened slightly before landfall 9 h later (Case and Gerrish 1988). Research aircraft observed Emily at maximum intensity, and although they generally remained within 60 km of the center in order to obtain optimum Doppler radar coverage, some of the longer radial legs show an outer wind maximum on the east side. The observations are not, however, good enough to determine whether a concentric eye occurred or played a role in Emily's development.

In Gilbert on 13 September 1988, the aircraft that extrapolated the record minimum sea-level pressure for an Atlantic hurricane (888 hPa, Willoughby et al. 1989) also observed formation of an outer eyewall. Seven hours later, the next aircraft observed that V_{max} had decreased from 80 m s^{-1} to <70 m s^{-1} and the secondary wind maximum, which coincided with a well-defined outer convective ring on radar, had strengthened to >45 m s^{-1}. It was in this concentric eye phase that Gilbert struck the Yucatan Peninsula, reemerging over the gulf the next day with the relict inner eye still visible on radar and $V_{max} < 50$ m s^{-1}. For the next two days as Gilbert crossed the Bay of Campeche to final landfall on the Mexican mainland, it had a flat wind profile with little intensity change, much like Gloria after its concentric eyewall. Clearly, Gilbert weakened as a result of the outer eyewall, but passage over land and the shallower oceanic mixed layer west of the Yucatan played an important role in the transformation of the vortex. A detailed analysis of Gilbert will appear separately.

6. Conclusions

Extensive observations show that convectively driven contracting maxima of the swirling wind con-

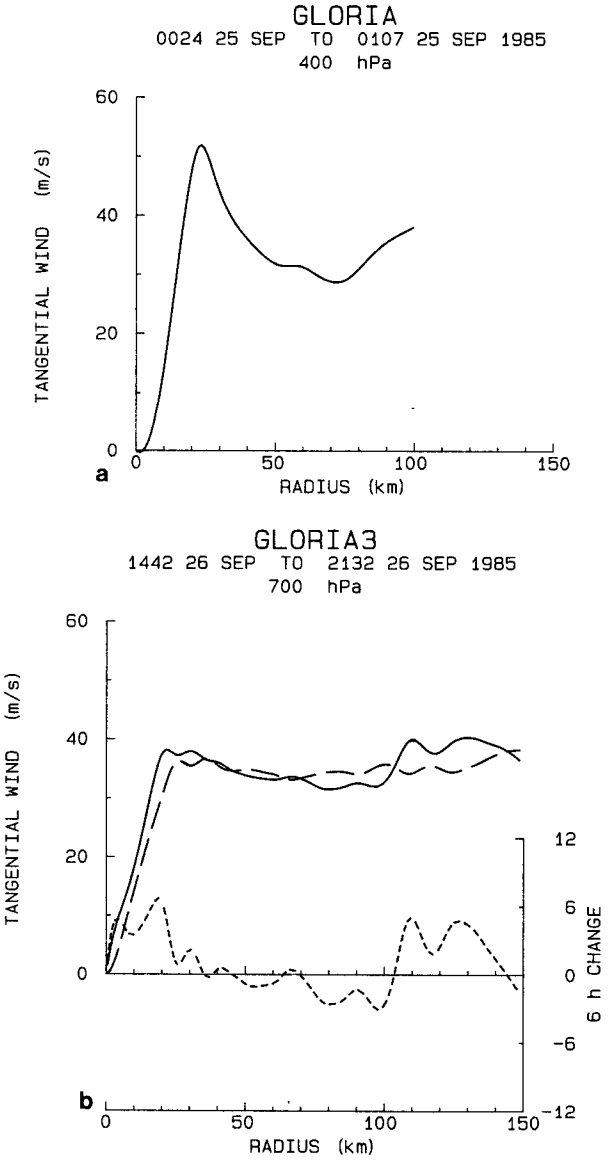

FIG. 24. The evolution of Hurricane Gloria: (a) the primary circulation with an outer wind maximum flight 850924I; (b) flat wind profile and slow temporal change during flight 850926H. The curves have the same meaning as in Fig. 2b, except tnat Fig. 24a shows no wind tendency.

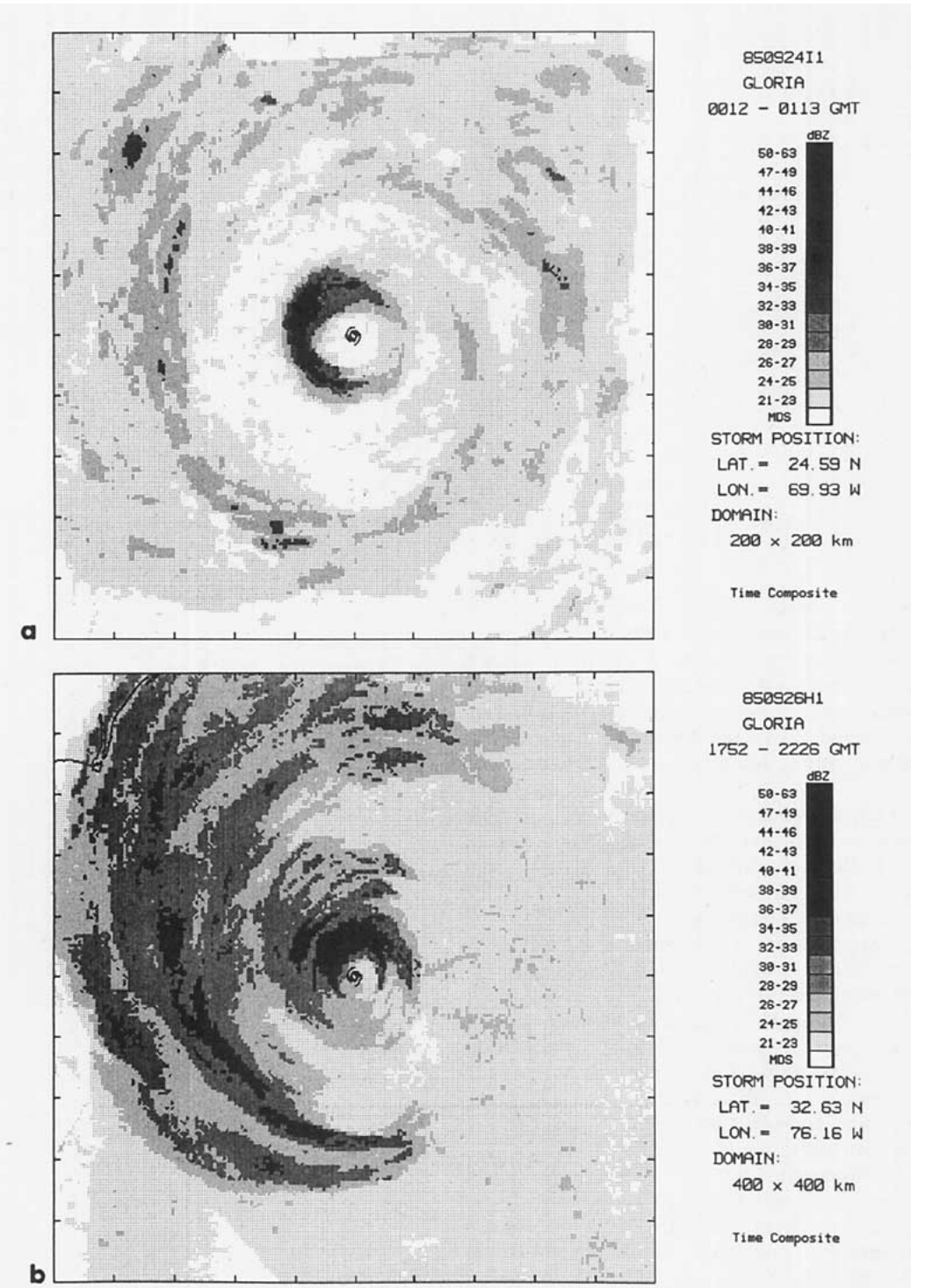

FIG. 25. Aircraft radar composites in Gloria: (a) concentric eyewall during flight 850924I and (b) inner eyewall and partial outer convective ring during flight 850926H. The reflectivity in the first composite is weaker than other cases because the aircraft flew above the 0° isotherm where the radar returns came largely from frozen hydrometeors.

stitute the primary mechanism for intensification of hurricanes. The peaked radial profiles of the swirling wind that characterize these features in rapidly strengthening hurricanes contrast with the flat profiles observed in slowly intensifying or weakening ones. On radar, the wind maxima coincide with convective rings,

annuli of reflectivity that form either by detachment from the inside of the principal band or by reorganization of spiral bands. The observed kinematics of the wind maxima's contraction agree with the theoretical response to imposed heating in a balanced vortex. In some intense, vigorously convective hurricanes, outer concentric rings form and supplant the preexistent eyewall, often provoking rises of central pressure and ultimately leading to flat wind profiles that characterize nonintensification.

In hurricanes with flat wind profiles and less vigorous convection, minor convective rings may form, persist for a time while contracting slowly, and ultimately dissipate with little effect on the vortex as a whole. In tropical storms or weak hurricanes, outbreaks of powerful asymmetric convection usually mark the start of intervals of relative quiescence. Asymmetric convection may also cause cyclone centers to move erratically some tens of kilometers in a few hours, in contrast with the loops induced by changes in the steering flow—such as passing troughs—which require about a pendulum day to complete.

The data from Hurricane Diana record a complete concentric eyewall replacement in detail: formation of the outer eyewall, contraction of the outer eyewall, destruction of the original eyewall, and weakening of the cyclone. The observations of Gloria provide a snapshot of the concentric eyewall and document the resulting weakened cyclone. Alicia formed a contracting outer eyewall, but moved ashore just as the inner eyewall began to weaken. Elena had a flat wind profile for much of its life and formed three transient minor convective rings. It had a peaked wind maximum only during the time when it interacted with a passing midlatitude trough. Observations of Emily are unclear as to whether or not the weakening before landfall on Hispaniola involved an outer eyewall, but Gilbert clearly weakened as a result of an outer eyewall before it struck the Yucatan. Thus, of six hurricanes with $V_{max} \geq 45$ m s^{-1} documented by detailed aircraft observations since 1983, two weakened through concentric eyewall cycles over the sea, two weakened a little through formation of an outer eyewall just before landfall, one escaped major structural change caused by a concentric eyewall, and in one the observations are inconclusive. All vigorously convective concentric eyewalls contracted, leading to destruction of the inner eyewall unless the hurricane moved ashore first. These observations, combined with those in Willoughby et al. (1982), show clearly that concentric eyewalls play a role in development of many, but not all, major hurricanes.

Three of the four confirmed outer eyewalls in this study formed near shore. This pattern may support the idea that topographic forcing initiates concentric eyewalls (Hawkins 1983), or it may reflect a bias toward landfall because the data were collected during reconnaissance of hurricanes that threatened shore. A limited number of case studies offer hope that at least some primary eyewalls have synoptic-scale precursors in low level surges (Molinari and Skubis 1985) or upper level angular momentum influxes (Molinari and Vollaro 1989). Diverse mechanisms for origin are by no means mutually exclusive if hurricanes "want" to organize their convection into rings—that is, if the convective ring structure is, in a sense, a normal mode or an attractor.

Acknowledgments. I want to express my thanks to everyone at the Hurricane Research Division and Aircraft Operations Center who participated in the research flights reported here; I have boundless admiration for the skill and stamina with which they flew the airplanes, kept the equipment working, and made the observations. I especially appreciate the help of Robert Burpee, the Hurricane Research Division's field program manager, and James McFadden, his counterpart at the Aircraft Operations Center. I also want to thank Neil Frank and Robert Sheets, former and current directors of the National Hurricane Center, whose cooperation facilitated research flights in conjunction with operational reconnaissance; Paul Leighton and Frank Marks, who prepared the radar imagery; William Barry and M. Edward Rahn, who did much of the computer programming and analysis of in situ data; Constance Arnhols, who provided editorial assistance; and John Gamache, Chris Landsea, and Frank Marks, whose comments on an earlier draft led to a much better paper.

REFERENCES

Case, R. A., 1986: Atlantic hurricane season of 1985. *Mon. Wea. Rev.*, **114,** 1390–1405.

——, and H. P. Gerrish, 1984: Atlantic hurricane season of 1983. *Mon. Wea. Rev.*, **112,** 1083–1092.

——, and ——, 1988: Atlantic hurricane season of 1987. *Mon. Wea. Rev.*, **116,** 939–949.

Eliassen, A., 1952: Slow thermally or frictionally controlled meridional circulation in a circular vortex. *Astrophys. Norv.*, **5,** 19–60.

Franklin, J. L., S. J. Lord and F. D. Marks, 1988: Dropwindsonde and radar observations of the eye of Hurricane Gloria (1985). *Mon. Wea. Rev.*, **116,** 1237–1244.

Gray, W. M., and D. J. Shea, 1973: The hurricane's inner core region. II. Thermal stability and dynamic characteristics. *J. Atmos. Sci.*, **30,** 1565–1576.

Hawkins, H. F., 1983: Hurricane Allen and island obstacles. *J. Atmos. Sci.*, **40,** 1360–1361.

Jorgensen, D. P., and P. T. Willis, 1982: A *Z-R* relationship for hurricanes. *J. Appl. Meteor.*, **21,** 356–366.

Lawrence, M. B., and G. B. Clark, 1985: Atlantic hurricane season of 1984. *Mon. Wea. Rev.*, **113,** 1228–1237.

Molinari, J., and S. Skubis, 1985: Evolution of the surface wind field in an intensifying tropical cyclone. *J. Atmos. Sci.*, **42,** 2856–2879.

——, and D. Vollaro, 1989: External influences on hurricane intensity. Part I: Outflow layer eddy angular momentum fluxes. *J. Atmos. Sci.*, **46,** 1093–1105.

Marks, F. D., 1985: Evolution of the structure of precipitation in Hurricane Allen (1980). *Mon. Wea. Rev.*, **113,** 909–930.

Neuman, S., and J. G. Boyd, 1962: Hurricane movement and variable location of high intensity spot in wall cloud radar echo. *Mon. Wea. Rev.*, **90,** 371–374.

Ooyama, K. V., 1987: Scale-controlled objective analysis. *Mon. Wea. Rev.*, **115,** 2479–2506.

Riehl, H., 1954: *Tropical Meteorology,* McGraw-Hill, 392 p.

Schubert, W. H., and J. J. Hack, 1982: Inertial stability and tropical cyclone development. *J. Atmos. Sci.*, **39,** 1687–1697.

Shapiro, L. J., and H. E. Willoughby, 1982: The response of balanced hurricanes to local sources of heat and momentum. *J. Atmos. Sci.*, **39,** 378–394.

Smith, R. K., 1981: The cyclostrophic adjustment of vortices with application to tropical cyclone modification. *J. Atmos. Sci.*, **38,** 2021–2030.

Velden, C. S., 1987: Satellite observation of Hurricane Elena (1985) using the VAS 6.7-μm "water vapor" channel. *Bull. Amer. Meteor. Soc.*, **68,** 210–215.

Willoughby, H. E., 1979: Forced secondary circulations in hurricanes. *J. Geophys. Res.*, **84,** 3173–3183.

——, 1990: Gradient balance in tropical cyclones. *J. Atmos. Sci.*, **47,** 265–274.

——, J. A. Clos and M. G. Shoreibah, 1982: Concentric eyewalls, secondary wind maxima, and the evolution of the hurricane vortex. *J. Atmos. Sci.*, **39,** 395–411.

——, and M. B. Chelmow, 1982: Objective determination of hurricane tracks from aircraft observations. *Mon. Wea. Rev.*, **110,** 1298–1305.

——, F. D. Marks and R. J. Feinberg, 1984: Stationary and moving convective bands in hurricanes. *J. Atmos. Sci.*, **41,** 3189–3211.

——, D. P. Jorgensen, R. A. Black and S. L. Rosenthal, 1985: Project STORMFURY: A scientific chronicle 1962–1983. *Bull. Amer. Meteor. Soc.*, **66,** cover and 505–514.

——, J. M. Masters and C. W. Landsea, 1989: A record minimum sea-level pressure observed in Hurricane Gilbert. *Mon. Wea. Rev.*, **117,** 2824–2828.